Targeting CaMKK2 Inhibits Actin Cytoskeletal Assembly to Suppress Cancer Metastasis

Debarati Mukherjee[1], Rebecca A. Previs[2], Corinne Haines[1], Muthana Al Abo[3], Patrick K. Juras[1], Kyle C. Strickland[4], Binita Chakraborty[1], Sandeep Artham[1], Regina S. Whitaker[2], Katherine Hebert[5], Jake Fontenot[6], Steven R. Patierno[3], Jennifer A. Freedman[3], Frank H. Lau[6], Matthew E. Burow[5], Ching-Yi Chang[1], and Donald P. McDonnell[1]

ABSTRACT

Triple-negative breast cancers (TNBC) tend to become invasive and metastatic at early stages in their development. Despite some treatment successes in early-stage localized TNBC, the rate of distant recurrence remains high, and long-term survival outcomes remain poor. In a search for new therapeutic targets for this disease, we observed that elevated expression of the serine/threonine kinase calcium/calmodulin (CaM)-dependent protein kinase kinase 2 (CaMKK2) is highly correlated with tumor invasiveness. In validation studies, genetic disruption of CaMKK2 expression or inhibition of its activity with small molecule inhibitors disrupted spontaneous metastatic outgrowth from primary tumors in murine xenograft models of TNBC. High-grade serous ovarian cancer (HGSOC), a high-risk, poor prognosis ovarian cancer subtype, shares many features with TNBC, and CaMKK2 inhibition effectively blocked metastatic progression in a validated xenograft model of this disease. Mechanistically, CaMKK2 increased the expression of the phosphodiesterase PDE1A, which hydrolyzed cyclic guanosine monophosphate (cGMP) to decrease the cGMP-dependent activity of protein kinase G1 (PKG1). Inhibition of PKG1 resulted in decreased phosphorylation of vasodilator-stimulated phosphoprotein (VASP), which in its hypophosphorylated state binds to and regulates F-actin assembly to facilitate cell movement. Together, these findings establish a targetable CaMKK2–PDE1A–PKG1–VASP signaling pathway that controls cancer cell motility and metastasis by impacting the actin cytoskeleton. Furthermore, it identifies CaMKK2 as a potential therapeutic target that can be exploited to restrict tumor invasiveness in patients diagnosed with early-stage TNBC or localized HGSOC.

Significance: CaMKK2 regulates actin cytoskeletal dynamics to promote tumor invasiveness and can be inhibited to suppress metastasis of breast and ovarian cancer, indicating CaMKK2 inhibition as a therapeutic strategy to arrest disease progression.

Introduction

Breast cancer has surpassed lung cancer as the leading cause of cancer incidence, with an estimated 2.3 million new cases in 2020, representing approximately 11.7% of all cancer cases worldwide (1). It remains the most common cause of cancer-associated deaths among women and is responsible for nearly 15% of all new cancer cases each year in the United States (2). Approximately 90% of all breast cancer related deaths can be attributed to metastasis (3). While the 5-year overall survival rate of patients with breast cancer without metastasis is now over 80% (4), it drops significantly (∼25%) for patients diagnosed with metastatic disease (5). Among the breast cancer subtypes 12% to 17% are classified as triple-negative breast cancer (TNBC; ref. 6). TNBC tumors are generally more aggressive and have a worse prognosis than other breast tumor subtypes. Early-stage patients with TNBC presenting with locally invasive, lymph node–positive disease are at a high risk of developing distant metastatic recurrence within 2 to 3 years from initial diagnosis. Despite advances in treatments for patients with early stage, locally advanced TNBC, most do not achieve a pathologic complete response (pCR) and 5-year recurrence rates remain approximately 80% (7, 8). The high rate of distant recurrence, even among women presenting with early-stage disease, reinforces the need to understand the fundamental molecular mechanisms that drive localized tumor cell invasion and distant metastasis in TNBC. It is anticipated that elucidation of the mechanisms underlying these processes will allow the identification of interventions that can significantly impact the invasiveness and metastatic potential of this cancer.

High-grade serous ovarian cancer (HGSOC) is a highly aggressive, poor prognosis malignancy that shares similar molecular phenotypes with TNBC in that both cancers exhibit frequent *TP53* mutations, inactivation of *BRCA1* and *BRCA2*, and mutations in *NF1* and *RB* (3). These cancers are also characterized by a high degree of genomic instability and deficiencies in homologous recombination (HR; refs. 3, 9). Indeed, reflecting their shared genetic characteristics, there are several ongoing clinical trials enrolling patients with either HGSOC or TNBC (ClinicalTrials.gov identifier: NCT01623349, ClinicalTrials.gov identifier: NCT00679783). Unfortunately, patients with HGSOC most often present with metastatic disease where treatment options are

[1]Department of Pharmacology and Cancer Biology, Duke University School of Medicine, Durham, North Carolina. [2]Department of Obstetrics and Gynecology, Division of Gynecologic Oncology, Duke University Medical Center, Durham, North Carolina. [3]Department of Medicine, Division of Medical Oncology, Duke University School of Medicine, Durham, North Carolina. [4]Department of Pathology, Duke University Medical Center, Durham, North Carolina. [5]Department of Medicine, Section of Hematology and Oncology, Tulane University School of Medicine, New Orleans, Louisiana. [6]Department of Surgery, Section of Plastic & Reconstructive Surgery, Louisiana State University Health Sciences Center, New Orleans, Louisiana.

Corresponding Author: Donald P. McDonnell, Duke University School of Medicine, B238 LSRC, 308 Research Drive, Box 3813, Durham, NC 27710. Phone: 919-684-6035; E-mail: donald.mcdonnell@duke.edu

Cancer Res 2023;83:2889–907

doi: 10.1158/0008-5472.CAN-22-1622

limited to cytoreductive surgery and chemotherapy followed by maintenance therapies such as bevacizumab and/or poly-ADP ribose polymerase inhibitors (10, 11). However, most patients will develop secondary metastases for which there are few therapeutic options, highlighting the clear unmet need for treatments that limit the metastatic progression of HGSOC (12). Given that HGSOC and TNBC are genetically similar cancers with high rates of postoperative distant recurrence, the addition of an anti-invasive therapy following primary surgery could be potentially incorporated into current treatment paradigms along with other maintenance therapies to provide significant survival benefit to both these patient cohorts.

Calcium/calmodulin (CaM)-dependent protein kinase kinase 2 (CaMKK2) is a serine/threonine kinase that couples a variety of external stimuli to intracellular pathways involved in the regulation of cell proliferation, survival, and metabolism (13). This enzyme was initially identified as a component of the calcium/calmodulin-dependent protein kinase (CaMK) cascade that is activated in response to elevated intracellular Ca^{2+}. However, CaMKK2 also exhibits significant activity independent of Ca^{2+}/calmodulin (CaM) binding (autonomous activity; refs. 13, 14). The most well-characterized downstream effectors of CaMKK2 activity are CaMKI, CaMKIV, and AMPKα (13, 15). CaMKK2 acts through CaMKI to activate ERK and CREB, which directly impacts neurite outgrowth in neuroblastoma and osteoclast differentiation during bone development (16, 17, 18). Furthermore, CaMKK2-CaMKI can regulate cytoskeletal architecture and actin-based motility in developing neurons (19). CaMKK2-dependent activation of CaMKIV directly controls liver cancer cell proliferation (20), and modulates the homeostatic functions of brain-derived serotonin (21). AMPKα functions as a key integrator/regulator of CaMKK2 activity, and this signaling axis regulates metabolic responses to energetic stress, particularly in the brain (22), liver (23), and adipose tissue (24). In addition to its role in maintaining whole body energy homeostasis, the CaMKK2–AMPK pathway can integrate cellular responses to cellular Ca^{2+} influxes to modulate anoikis (25), autophagy (26), cell viability/survival (27), micropinocytosis (28), and cellular migration (29).

CaMKK2 is aberrantly overexpressed in a number of cancers, and its role in primary tumor models of prostate cancer (30), lung cancer (25), glioblastoma (31), ovarian cancer (32), renal cell carcinoma (26), and pancreatic cancer (28) have been explored. We recently reported that CaMKK2 is strongly expressed within cancer cells and stromal cells in breast tumors and that its elevated expression is correlated with more aggressive TNBC (33). Previously, we demonstrated that CaMKK2 activity within myeloid cells supports tumor growth by reprogramming the tumor immune microenvironment (33). However, the importance of CaMKK2 expressed within cancer cells on tumor pathobiology has not been established. Interestingly, CaMKK2 was recently implicated as an upstream regulator of actin polymerization and stress fiber assembly in osteoclasts (34). The presence of a robust network of thick intracellular actin stress fibers is a hallmark of migrating cells and provides the force necessary to trigger cellular motility (35). Indeed, CaMKK2 action has previously been shown to regulate actin-based cellular motility in developing neurons (19). These observations, together with the finding that CaMKK2 is aberrantly overexpressed in highly metastatic tumors (33), prompted us to probe if and how CaMKK2 action regulates tumor cell motility, migration, and metastatic dissemination from primary tumors. We found that depletion/inhibition of CaMKK2 disrupted actin cytoskeleton organization in cancer cells, which resulted in decreased spontaneous metastasis in murine xenograft models of TNBC. We also determined that inhibition of CaMKK2 activity decreased metastasis in a validated model of HGSOC. This work highlights the potential utility of recently developed, highly specific, CaMKK2 inhibitors as treatments for patients with TNBC or HGSOC.

Materials and Methods

Reagents

STO-609 and GSK1901320 (referred to as GSKi) were synthesized at the Duke University Small Molecule Synthesis Facility. Ionomycin (catalog #10004974) was obtained from Cayman Chemicals and solubilized in DMSO at room temperature, sterile filtered (0.2 μmol/L), and stored at −20°C. The pan-PDE inhibitor, IBMX (catalog #BML-PD140) and PDE1-specific inhibitor, vinpocetine (catalog #BML-PD185) were purchased from Enzo Life Sciences. Sildenafil (catalog #10008671) was obtained from Cayman Chemicals. The nitric oxide synthase (NOS) inhibitors, N_ω-Nitro-L-arginine (L-NNA; catalog #N5501) and N_ω-Nitro-L-arginine methyl ester hydrochloride (L-NAME; catalog #N5751) were both obtained from Millipore Sigma and solubilized in 1 mol/L HCL and dH_2O, respectively. To stain filamentous actin, rhodamine-phalloidin (catalog #R415) was purchased from Thermo Fisher Scientific, dissolved in methanol, and stored at −20°C. The small-molecule PKG inhibitors, RKRARKE (catalog #370654) and KT5823 (catalog #K1388) were both obtained from Millipore Sigma.

Cells and cell culture conditions

Luciferase-labeled lung-trophic MDA-MB-231-4175 cells were kindly provided by Dr. Joan Massague (Memorial Sloan Kettering Cancer Center, New York, NY). 4T1, BT-20, and HCC1954 cells were purchased from ATCC. SKOV3ip1 and HOC7 cells were kindly provided by Drs. Guillermo Armaiz-Pena (Ponce Health Sciences University, Ponce, Puerto Rico) and Arktak Tovmasyan (Duke University, Durham, NC), respectively. MDA-MB-231-4175, BT20, and 4T1 cells were maintained in DMEM. HCC1954, HOC7, and SKOV3iP1 were grown in RPMI1640 media. DMEM and RPMI media were supplemented with 8% fetal bovine serum (FBS, Sigma), 1 mmol/L sodium pyruvate, and 0.1 mmol/L nonessential amino acids (Thermo Fisher Scientific). All cells were cultured in a humidified incubator at 37°C with 5% CO_2. For experiments with ionomycin, cells were grown until 90% confluent and the culture media was then replaced with Hanks' Balanced Salt Solution (HBSS; Gibco) supplemented $MgCL_2$ (1 mmol/L) for 15 minutes prior to ionomycin exposure. The cells were then treated with either DMSO or ionomycin (1 μmol/L) with $CaCL_2$ (1 mmol/L) for varying time periods (as indicated) before harvesting the cells for downstream processing.

Generation of CaMKK2 knockout cell lines

sgRNAs targeting specific sequences at the N-terminal end of the *CaMKK2* gene were purchased from Synthego Corp. For each sgRNA, a ribonucleoprotein (RNP) complex was formed with the Cas9 2NLS nuclease (Synthego), at a sgRNA: Cas9 ratio of 6:1. MDA-MB-231-4175 cells were seeded at 8×10^4 cells/mL and transfected with the RNP complex using Lipofectamine CRISPRMAX transfection reagent (catalog #CMAX00008, Thermo Fisher Scientific). Five to 6 days posttransfection, cells were plated for single-cell isolation in 96-well plates at a limiting dilution of 0.6 cells/well. Single-cell clones were allowed to expand and clones with successful knockout of CaMKK2 were identified directly by immunoblotting. One random clone was selected for each of sgRNA #1, #2, and #3, as indicated, and

used for experiments. The sequences of all sgRNAs used in the study are included in Supplementary Table SI.

Generation of CaMKK2/PDE1A overexpression cell lines in CaMKK2-KO cells

Lentiviral constructs expressing wild-type CaMKK2 or PDE1A were created by shuttling CaMKK2 or PDE1A from the pDONR221 vector backbone to pLenti-CMV-puro-DEST (Addgene) using Gateway cloning. All plasmids were confirmed via restriction digests and/or Sanger sequencing. CaMKK2 addback cell lines and PDE1A overexpression in CaMKK2-KO background were generated by infecting the MDA-MB-231-4175 CaMKK2 knockout clones (KK2-KO #1 and KK2-KO #2) with lentiviruses expressing wild-type CaMKK2 or wildtype PDE1A or empty vector (control). Transduced cells were selected using puromycin (1 μg/mL). Addback was confirmed by immunoblot analysis.

siRNA transfection

MDA-MB-231-4175 (50,000 cells/mL), BT-20 (50,000 cells/mL), HCC1954 (60,000 cells/mL), and HOC7 (75,000 cells/mL) cells were transfected with either control siRNAs (catalog #12935146, Thermo Fisher Scientific; catalog #SIC001, Millipore Sigma) or CaMKK2 siRNAs (50 nmol/L; catalog #10620318, Thermo Fisher Scientific) using the DharmaFECT 1 transfection agent (catalog #T-2001–03, Dharmacon) according to the manufacturer's instruction. Cells were collected for downstream analysis after 48 hours (36) or 72 hours posttransfection (protein). The sequences of the siRNAs used are included in Supplementary Table SII.

Cell proliferation assay

Control clones (Ctrl #1, Ctrl #3) and CaMKK2-KO clones (KK2-KO #1, KK2-KO #2, and KK2-KO #3) derived from parental MDA-MB-231 cells, were plated in 96-well plates with 5,000 cells seeded in each well and cultured in 8% FBS-containing media. Cells were collected on day 0 (day after cells were seeded), day 2, and day 4, as indicated. DNA content was measured using Hoechst 33258 (Sigma). Plate reader (TECAN Spark) was used to evaluate the fluorescence intensity, which was read at an excitation of 346 nm and emission of 460 nm. Data represents three individual experiments with biological replicates.

Migration/invasion assays

To evaluate cellular migration, transwell inserts suited for 24-well plates were used. Cells were serum-starved overnight and seeded in transwell inserts (8 μm pore size, catalog #3422, Corning) in 250 μL of serum-starved media (0.5% FBS). The lower well contained 800 μL of full serum media (8% FBS). The cells were allowed to migrate in a humidified incubator at 37°C with 5% CO2 for a duration of 8 hours unless otherwise indicated in individual experiments. To evaluate invasiveness, cells were seeded on Biocoat invasion chambers with 8 μm pore size PET membrane precoated with extracellular matrix proteins (catalog #354480, Corning). Invasion assays were conducted as per the manufacturer's protocol using the same seeding conditions as in transwell migration. For both migration and invasion assays, the transwell/invasion chambers were collected at the end of the incubation period and the migrated cells were fixed with 4% paraformaldehyde for 1 hour at 4°C followed by staining with 0.1% crystal violet for 1 hour at room temperature. Nine images per insert were photographed under a microscope at ×10 magnification, with at least three technical repeats per experiment. Total number of migrated/invaded cells were measured by ImageJ. For migration/invasion experiments with CaMKK2 inhibitors, cells were first treated with Vehicle or STO-609 (10 μmol/L) or GSKi (1 μmol/L) in 8% FBS-containing media for 24 hours and then again in serum-starved media for the next 24 hours before the cells were harvested for experiments (total treatment time: 48 hours). Wound healing assays were conducting in 12-well plates whereby cells were allowed to grow to a confluent monolayer before serum-starvation overnight. Three vertical scratches were then introduced using a p200 pipette tip and at least 12 points (per condition) were marked for monitoring. The media was changed to remove displaced cells and images were photographed at 0 (immediately after scratches were introduced), 48, and 60 hours, as indicated. The rate of migration was evaluated using ImageJ. Specifically, percentage area migrated was calculated by $X = [(OAT1 - OAT2)/OAT1] \times 100$, where X = Percentage area migrated; OAT1 = Open area (scratch width) at Time1 (earlier time point), OAT2 = Open area (scratch width) at Time2 (later time point).

Animal studies

Six-week-old Athymic nude-*Foxn1*^{nu} mice were purchased from Envigo. The mice were housed in secure animal facility cages under pathogen-free conditions on a 12-hour light/dark cycle at a temperature of approximately 25°C and 70% humidity. Mice had *ad libitum* access to food and water. All xenograft procedures were approved by the Duke University Institutional Animal Care and Use Committee (IACUC). To study spontaneous metastasis from the primary tumor, luciferase-labeled cells (MDA-MB-231-4175: 1×10^6 cells per mouse; 4T1: 5,00,000 cells per mouse; suspended in HBSS/Matrigel, 1:1) were inoculated orthotopically into the mammary fat pads of 8-week-old female athymic nude mice. Mice were monitored daily, and tumor volume was measured with electronic calipers using the formula $V = L \times (W \times W)/2$ (L = length; W = width). Each mouse in each group was euthanized when the tumor reached a maximum size of 2,000 to 2,500 mm^3 as specified by the Duke IACUC protocol. For mice injected with MDA-MB-231-4175 cells, the animals were injected with D-luciferin prior to euthanizing. The secondary organs (liver, lungs) were then collected and micrometastasis was visualized by bioluminescent imaging *ex vivo* using the IVIS Lumina XR In Vivo Imaging System (PerkinElmer). For xenograft studies using 4T1 cells, the secondary organs were collected at the end of the study and metastatic nodules in the lung were visualized and counted *ex vivo*. Experimental metastasis using the MDA-MB-231-4175 cellular model was studied by injecting viable luciferase-labeled metastatic cells (5,00,000; suspended in ice-cold 200 μL HBSS) into the lateral tail veins of 8-week-old athymic nude mice. The extent of lung metastasis was monitored by bioluminescent imaging of the live animals using the IVIS Lumina XR In Vivo Imaging System (PerkinElmer). Mice were euthanized at indicated time points. For *in vivo* experiments involving drug treatments, 8-week-old athymic nude mice were orthotopically injected with parental MDA-MB-231-4175 cells (1.5×10^6 cells/mouse) into the mammary fat pad, as described above. Therapeutic dosing was started 5 days after tumor cell injection at a starting tumor size of 50 mm^3 approx. The mice were dosed with vehicle (PEG-8, PolyethyleneGylcol 400; Spectrum Chemical MFG Corp), STO-609 (40 μmol/kg body weight), or GSKi (10 μmol/kg body weight) via intraperitoneal injections every third day. Tumor size was monitored throughout the study and micrometastasis in secondary organs (lung, liver) was evaluated as described above. For *in vivo* metastasis experiments with the HGSOC model, SKOV3ip1 cells (1×10^6 cells in 200 μL of HBSS) were injected intraperitoneally into 9-week-old female athymic nude mice (Charles River Laboratories). Mice were treated

via intraperitoneal injection with vehicle (PEG-8, PolyethyleneGylcol 400; Spectrum Chemical MFG Corp) or STO-609 (MedKoo Biosciences, Inc.; 40 μmol/kg) twice weekly. Once mice in any group became moribund, all mice were sacrificed and necropsied. Metastatic burden was harvested, weighed, and location of metastatic nodules were recorded. Statistical analyses were performed by Student *t* test or two-way ANOVA followed by a Bonferroni multiple comparison test.

Sandwiched white adipose tissue preparation

Control cells (Ctrl#1, Ctrl#3) and CaMKK2-KO cells (KK-KO#1, KK2-KO#2) were stained with Cell Brite Green Dye at 37°C for 45 minutes and mixed with freshly isolated minced human breast tissue in individual 3.5 cm Sandwiched white adipose tissue (SWAT) Petri dish as described previously (37, 38). The SWAT dishes were incubated overnight to allow the system to stabilize. Media was changed after 24 hours, and the SWAT systems received fresh media daily until the end of the experiment.

Time-lapse video and measurement of 3D cell movement

Using the Nikon Elements Software, a workflow was created to capture fluorescence microscopy and brightfield images every 5 minutes over 6 hours yielding a total of 73 frames. Each sample (both control lines and both CaMKK2 knockout lines) were captured using fluorescence only, followed by merged fluorescence and brightfield images. Each SWAT petri dish was then transferred sterilely to the Nikon scope top incubator and fixed in place. The incubator was set to 37°C and 5% CO_2 for all videos. Using FITC and brightfield lenses, specific areas of interest were selected that included both easily identifiable adipocytes and several of the dyed cancer cells. Magnification was adjusted to ×20, and autoexposure for each field type was adjusted to provide better picture quality. Each SWAT sample was filmed for a total of 12 hours, and the resulting videos were given scale bars, exported, and compressed to AVI format. Each video is approximately 14 seconds long (5 fps). AVI files were opened using the ImageJ software, and the tracking plugin MTrackJ was loaded through which specific cells were marked and traced through every frame of a given AVI file to generate a relative measurement of cell movement given in pixel length. Each track is represented by different colors and numbers for easy identification. Statistical analyses to evaluate differences in 3D movement of cells were performed by Student *t* test.

Immunoblotting and quantitative PCR

Cells were washed three times with 2 mL of ice-cold PBS, snap-frozen and lysed with 0.15 mL of phospho-RIPA lysis buffer (Tris-HCl pH 7.5, 50 mmol/L; NaCl, 150 mmol/L; NP-40, 1%; Sodium deoxycholate, 0.5%; SDS, 0.05%; EDTA, 5 mmol/L; sodium fluoride, 50 mmol/L; sodium pyrophosphate, 15 mmol/L; glycerophosphate, 10 mmol/L; sodium orthovanadate, 1 mmol/L) with protease inhibitor cocktail (Millipore-Sigma, P-8340). Twenty-five micrograms of lysates were denatured and resolved by SDS-PAGE. Proteins were transferred to Odyssey Nitrocellulose Membrane (catalog #926–31092, LI-COR Biosciences). Primary antibodies used were anti-CaMKK2 (MO1, clone 1A11, 1:2,000, catalog #H00010645-M01, Abnova); anti-phospho AMPKα (Thr 172; 1:1,000, catalog #2531, Cell Signaling Technology); anti-AMPKα (1:500, catalog #2532, Cell Signaling Technology); anti-phospho-VASP (Ser239; 1:1,000, clone 16C2, catalog #05–611, Millipore Sigma); anti-phospho-VASP (Ser157; 1:1,000, catalog #3111, Cell Signaling Technology); anti-VASP (1:2,000, catalog #HPA005724, Atlas Antibodies); anti-PDE1A (1:500, catalog #PD1A-101AP, FabGennix); anti-PDE5 (1:1,000, catalog #2395, Cell Signaling Technology); anti-PDE1C, 1:2,000, catalog #ab14602, Abcam); anti-Actin (1:10,000, 8H10D10, catalog #3700, Cell Signaling Technology). Secondary antibodies used were HRP-conjugated anti-mouse IgG (1:5,000 catalog #1706516) and anti-rabbit IgG (1:5,000; catalog #1706515), Bio-Rad, and protein bands were visualized by Western Lightning Plus ECL System (catalog #ORT2655 and ORT2755, PerkinElmer). Immunoblots shown are representative of at least two individual experiments unless otherwise indicated. For quantitative PCR, RNA was isolated using RNA Aqueous Micro Kit (catalog #1931, Ambion) followed by cDNA synthesis using an iScript cDNA Synthesis Kit (catalog #170–7691). Quantitative amplification was performed using Sybr Green (catalog #1725124, Bio-Rad) and a CFX-384 Real Time PCR detection system. Primers used to amplify the *PDE1A* gene are 5′-GAG TCT TCC CTC AGC TTT GT-3′ (forward) and 5′-TTT CAG TCT GTT CTC CTG TAA GAT-3′ (reverse).

Kaplan–Meier survival plot

To generate the Kaplan–Meier plots (https://kmplot.com) in **Fig. 1**, the parameters were set as follows: the probe to "CaMKK2 210787_s_at," the time to "(months): 180," the cutoff to "Upper quartile," the survival to "OS (overall survival)," and the PAM50 Subtype to "Basal, Luminal A, Luminal B, and HER2+." As of October 29, 2021, the number of patients included in KMplot analysis was 1,879. The survival data were downloaded as text files and used to draw the survival plots using Survminer R package (version 0.4.9).

Gene signature analysis

The Cancer Genome Atlas (TCGA) aggregate expression datasets for breast cancer were retrieved from the NCI Genomic Data Commons and processed using TCGAbiolinks (version 2.16.4) and Summarized Experiment (version 1.18.2) R packages. The samples' definition and PAM50 subtype were downloaded alongside the expression datasets. Tumor samples without PAM50 annotation were excluded. The number of samples included in the downstream analysis by definition: 1,072 primary solid tumor and 113 normal. Normal samples are designated as normal-adjacent. The number of samples by PAM50 subtyping: 189 Basal, 82 Her2, 206 LumB, 555 LumA, and 40 normal-like. EdgeR R package (version 3.30.3) was employed to normalize the RNAseq raw count for the library depth. A matrix using samples definition was designed, and the raw count and the normalization factor was calculated for normalization. Gene signature analysis was performed using the Gene Set Variation Analysis (GSVA) R package (BMC Bioinformatics, 14, 7. doi: 10.1186/1471–2105–14–7). The indicated gene sets were defined and the score in each sample was calculated. The method in the GSVA analysis were set to "gsva," and the kcdf option to "Gaussian." When comparing the scores of the gene sets between CAMKK2-high or CAMKK2-low expressing samples within different PAM50 subtypes, Wilcoxon signed rank test was used to calculate the *P* values. The box plots and the scattered plots were drawn using ggplot2 (version 3.3.5).

Analyses of human HGSOC correlates

We evaluated information from 62 patients diagnosed with advanced stage high-grade serous ovarian, fallopian tube or primary peritoneal cancer who were chemotherapy naïve. Human tissues were banked after written informed consent was obtained from each patient for the Duke University School of Medicine Ovarian Cancer Research Biobank under IRB protocol ID Pro00013710 (Banking Normal and Malignant Gynecologic Tissues Removed at Surgery). All studies were conducted in accordance with recognized ethical guidelines. Tissues were bio-banked in formalin-fixed paraffin-embedded (FFPE)

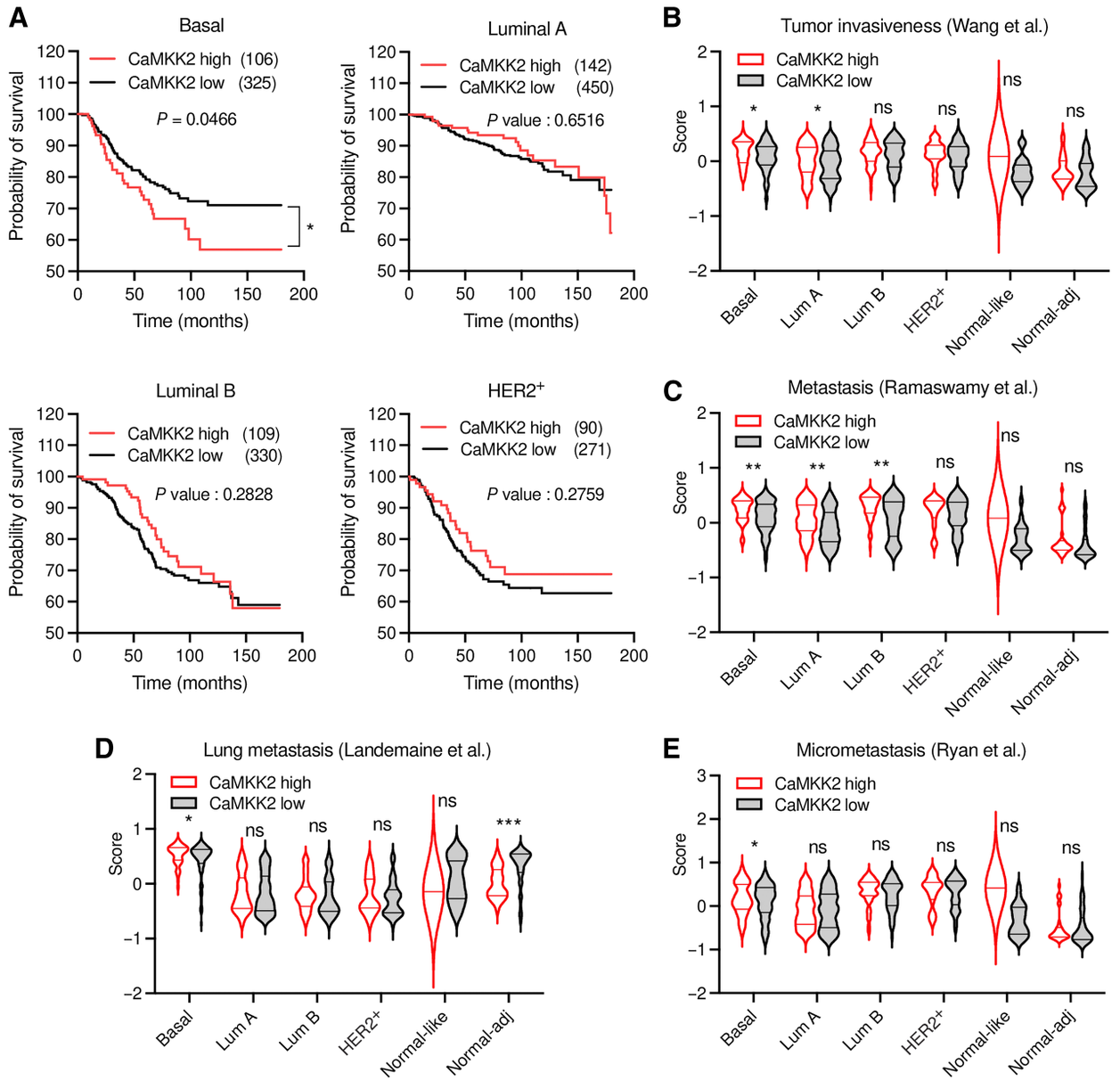

Figure 1.

Clinical relevance of CaMKK2 in metastatic TNBC. **A,** Kaplan–Meier plots showing the association between *CaMKK2* level and the overall survival of patients with basal ($n = 431$), luminal A ($n = 592$), luminal B ($n = 439$), or Her2$^+$ ($n = 361$) tumor subtypes. Patients were grouped into CaMMK2-high or -low by upper quartile (lower or higher than 75th percentile). The *x*-axis shows time in months, and the *y*-axis shows the overall survival probability. Plots were generated using KM-plotter (https://kmplot.com), **B–E,** Violin plots depicting the score for the gene signatures published in the indicated articles (36, 40, 41, 42). Samples were grouped into CaMMK2-high or -low by quartiles (equal or less than 25th percentile and equal or greater than 75th percentile). The *x*-axis shows breast cancer subtypes, and the *y*-axis shows the score between −1 and 1. Data, mean ± SEM. *, $P < 0.05$; **, $P < 0.01$; ***, $P < 0.005$; ns, nonsignificant; by Student *t* test (**B–E**) and log-rank test (**A**).

blocks. Histologic diagnoses were confirmed by a board-certified anatomic pathologist with experience in gynecologic pathology (K. C. Strickland). Clinicopathologic records were retrieved and stored in a database. The study was approved by the Institutional Review Board (IRB Pro00013710). After routine deparaffinization in xylene, rehydration, and inhibition of endogenous peroxidase activity with 3% hydrogen peroxidase, sections were exposed to heat-induced epitope retrieval (HIER) with the Decloaking Chamber (Biocare Medical) in Citra buffer (pH 6.0). After blocking with Background Terminator (Biocare Medical), the sections were incubated with rabbit anti-human antibody directed against CaMKK2 (HPA017389, Sigma) at 1:500, overnight at 4°C. This was followed by incubation with 4 Plus Universal Detection system (Biocare Medical), a universal affinity purified biotinylated secondary antibody, which is bound to a

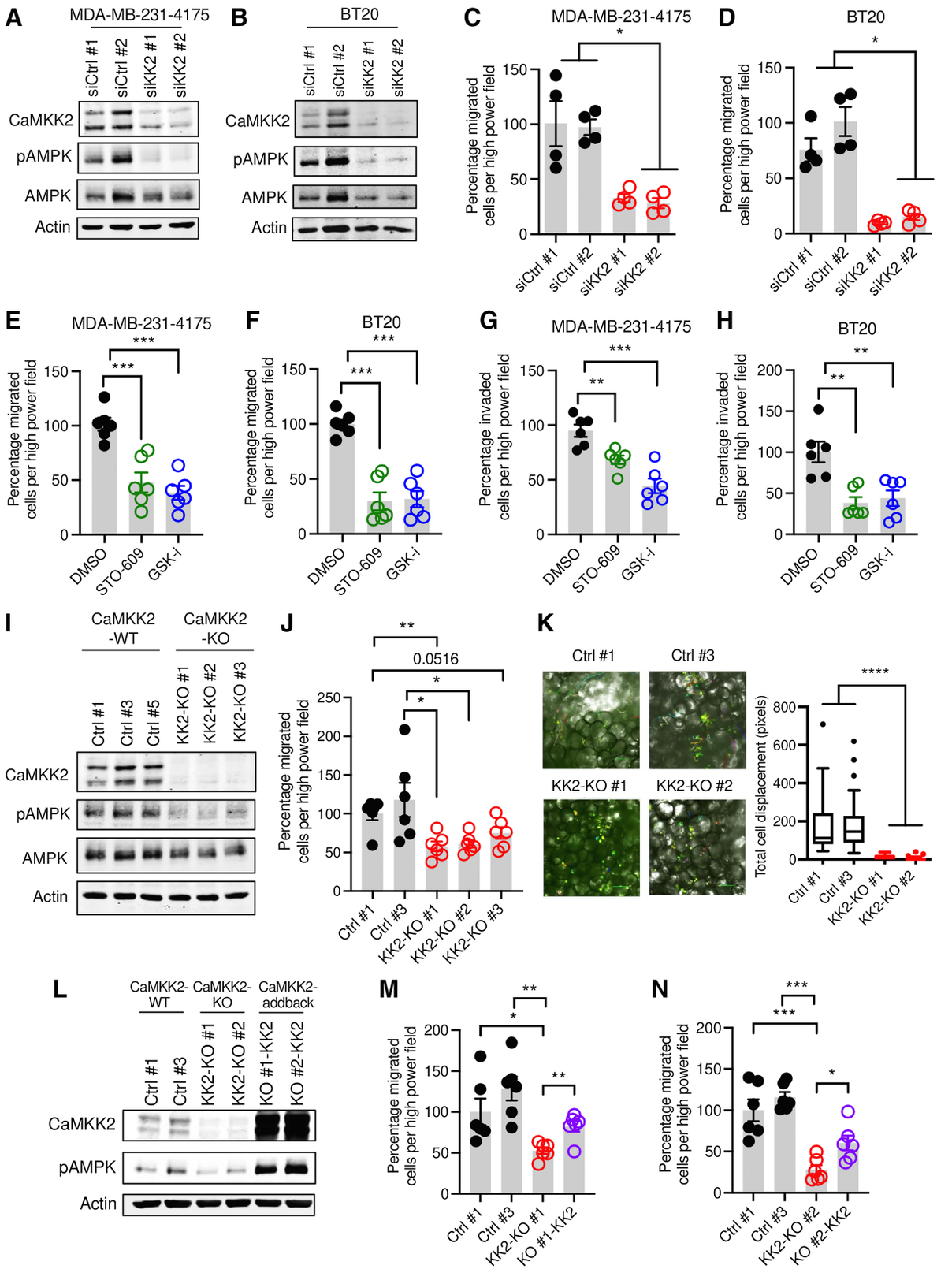
A
MDA-MB-231-4175
siCtrl #1
siCtrl #2
siKK2 #1
siKK2 #2
CaMKK2
pAMPK
AMPK
Actin
B
BT20
C
MDA-MB-231-4175
Percentage migrated cells per high power field
D
BT20
E
MDA-MB-231-4175
DMSO
STO-609
GSK-i
F
BT20
G
MDA-MB-231-4175
Percentage invaded cells per high power field
H
BT20
I
CaMKK2 -WT
CaMKK2 -KO
Ctrl #1
Ctrl #3
Ctrl #5
KK2-KO #1
KK2-KO #2
KK2-KO #3
J
0.0516
K
Ctrl #1
Ctrl #3
KK2-KO #1
KK2-KO #2
Total cell displacement (pixels)
L
CaMKK2- WT
CaMKK2- KO
CaMKK2- addback
KO #1-KK2
KO #2-KK2
M
N

horseradish peroxidase (HRP)–labeled streptavidin. The chromagen/substrate was applied to visualize the location and intensity of the protein of interest, and slides were counterstained with hematoxylin. Protein expression of CaMKK2 was evaluated using immunohistochemistry. Intensity of staining was reported using a semi-quantitative 4-part scale, as shown in the figure. Time-to-event analyses were based on the Kaplan–Meier method, and events were compared using the log-rank (Mantel–Cox) test.

Statistical analysis

Statistical analysis was performed with GraphPad Prism 8.0 (GraphPad Software), using either a two-tailed Student *t* test or 1- or 2-way ANOVA. For both 1-way and 2-way ANOVAs, a posttest analysis was performed using Bonferroni multiple correction. The number of replicates is indicated in the figure legends. A *P* value of less than 0.05 was considered statistically significant.

Study approval

All animal experiments were performed according to guidelines established and approved by the IACUC of Duke University.

Data and materials availability

TCGA aggregate expression datasets for breast cancer were obtained from the NCI Genomic Data Commons at https://gdc.cancer.gov/. All other raw data generated in this study are available upon request from the corresponding author.

Results

Elevated expression of CaMKK2 is associated with aggressive phenotypes and poor outcomes in patients with basal subtypes of breast cancer

Previously, we determined that the expression of CaMKK2 was elevated in invasive TNBC (33) and now report that higher expression of this enzyme is associated with reduced overall survival in patients with the basal subtype of breast tumors (**Fig. 1A**; top left). No differences in overall survival among patients with either luminal or $HER2^+$ disease was observed. Basal tumors are immunohistochemically defined by the lack of expression of the estrogen receptor (ER), progesterone receptor (PR), or HER2 with TNBCs representing a large fraction of cancers exhibiting the basal-like molecular subtype (39). Interestingly, validated gene signatures predicting increased tumor cell motility and invasiveness (40) and spontaneous metastatic potential from solid tumors (41) were found to be associated with elevated CaMKK2 expression in tumors from patients with basal-like or luminal disease (**Fig. 1B** and **C**). Furthermore, a well-validated 6-gene signature that predicts the occurrence of lung metastasis from primary breast tumors (42) was found to be significantly upregulated in basal tumors with high CaMKK2 expression (**Fig. 1D**). Finally, CaMKK2-high basal tumors (but not other tumor subtypes) showed significantly increased aggregate expression of a well-validated molecular signature that predicts micrometastatic outgrowth from primary breast tumors (**Fig. 1E**; ref. 36). Taken together, these results suggest that increased expression of CaMKK2 in primary tumors may be a key determinant of increased invasiveness and metastatic capacity in breast cancer, especially in patients with hormone receptor–negative, basal subtype(s) of this disease.

Depletion of CaMKK2 impairs the migratory potential of breast cancer cells

To directly probe the cancer cell intrinsic role(s) of CaMKK2 on tumor cell invasiveness and metastasis in TNBC, we assessed the impact of inhibiting CaMKK2 expression and activity in three cellular models of this disease: MDA-MB-231-4175, BT-20, and HCC1954. Changes in AMPK phosphorylation was used as a biomarker to assess the degree of CaMKK2 inhibition achieved. Transient siRNA-dependent knockdown of CaMKK2 expression in all three cell lines (**Fig. 2A** and **B**; Supplementary Fig. S1A) inhibited cell migration when compared to controls (**Fig. 2C** and **D**; Supplementary Fig. S1B). Similar outcomes were observed in cells treated with STO-609 (a commercially available CaMKK2 inhibitor), or GSK1901320 (GSKi; a highly selective CaMKK2 inhibitor; **Fig. 2E** and **F**; Supplementary Fig. S1C; ref. 33). Furthermore, inhibition of CaMKK2 activity reduced the invasiveness of both MDA-MB-231-4175 (**Fig. 2G**) and BT-20 cells (**Fig. 2H**). The loss of CaMKK2 expression or activity also inhibited the migration of HOC7 cells, a cellular model of ovarian cancer, indicating that the role of CaMKK2 in supporting cancer cell motility and migration is not restricted to breast cancers (Supplementary Fig. S1D and S1E).

To directly assess the role of CaMKK2 in migration and metastatic potential, we used CRISPR/Cas9-based genome editing to stably knock out CaMKK2 expression in highly metastatic MDA-MB-231-4175 cells. Four separate sg-RNAs (sg-RNA #A, #B, #C, and #D) targeting specific sequences at the 5′ end of the CaMKK2 coding region were used (Supplementary Fig. S1F, in red). Interestingly, these sgRNAs failed to abolish the lower band of the CaMKK2 doublet that is found in most cells (Supplementary Fig. S1G). We identified a potential cryptic translation initiation sequence approximately 150 bp downstream from the primary start site. Using sg-RNAs designed to specifically target sequences downstream from this site (sgRNA #1, #2, and #3; Supplementary Fig. S1F, in green), we were able to successfully abolish both CaMKK2 variants (Supplementary Fig. S1H). Following clonal expansion, a single CaMKK2-KO clone was randomly selected corresponding to each of the three sgRNAs #1, #2, and #3. Loss of CaMKK2

Figure 2.

Ablation of CaMKK2 impairs migration in invasive breast cancer cells. **A** and **B,** Representative blots showing knockdown of CaMKK2 in MDA-MB-231-4175 (**A**) and BT-20 cells (**B**). MDA-MB-231-4175 and BT-20 cells were transfected with either control siRNAs (siCtrl #1, siCtrl #2) or siRNAs targeting CaMKK2 (siKK2 #1, siKK2 #2). Forty-eight hours posttransfection, cells were harvested and immunoblots were used to analyze CaMKK2 and phospho-AMPKα (T172) expression. **C** and **D,** CaMKK2 knockdown impaired migration of MDA-MB-231-4175 cells (**C**) and BT-20 cells (**D**) *in vitro.* Data plotted as mean ± SEM; $n = 6$ random fields measurements from four individual experiments. **E** and **F,** Treatment with STO-609 (10 μmol/L; 48 hours) and GSKi (1 μmol/L; 48 hours) reduced migration of MDA-MB-231–4175 cells (**E**) and BT20 cells (**F**). Data plotted as mean ± SEM; $n = 9$ random fields measurements from two individual experiments done in triplicate. **G** and **H,** STO-609 (10 μmol/L; 48 hours) and GSKi (1 μmol/L; 48 hours) treatment reduced invasiveness in MDA-MB-231-4175 cells (**G**) and BT20 cells (**H**) *in vitro*. Data plotted as mean ± SEM; $n = 4$–5 random fields measurements from three individual experiments done in duplicate, **I**, Representative blots confirming CRISPR-mediated knockout of CaMKK2 in MDA-MB-231-4175 cells (see also Supplementary Fig. S1H), **J,** CRISPR-mediated ablation of CaMKK2 reduced migration in CaMKK2-KO clones *in vitro*, Data plotted as mean ± SEM; $n = 4$–5 random fields measurements from three individual experiments done in duplicate. **K,** Depletion of CaMKK2 reduced cellular movement in MDA-MB-231-4175 cells cultured with fresh human breast tissue. Fluorescence microscopy and brightfield images were captured every 5 minutes over 6 hours to track cellular movement (see also Supplementary Videos S1–S4). **L,** Representative blots confirming addback of CaMKK2 expression in CaMKK2-KO clones #1 and #2. **M** and **N,** Overexpression of CaMKK2 rescues migratory capability in both CaMKK2 KO clones. Data are plotted as mean ± SEM; $n = 4$–5 random fields measurements from three individual experiments done in duplicate. *, $P < 0.05$; **, $P < 0.01$; ***, $P < 0.005$; ****, $P < 0.001$. *P* values were calculated using unpaired Student *t* test.

expression and downstream function (AMPK phosphorylation) was confirmed in all three CaMMK2-KO cell clones (hereafter referred to as KK2-KO #1, KK2-KO #2, and KK2-KO #3; **Fig. 2I**). Whereas ablation of CaMKK2 did not impact cell proliferation (Supplementary Fig. S1I), it significantly reduced the migratory capability of cells (**Fig. 2J**; Supplementary Fig. S1J). This was confirmed using the SWAT preparation technique (37, 38) whereby two control clones and two CaMKK2-KO clones were mixed with freshly minced human breast tissue (adipocytes) to mimic the three-dimensional, multicellular microenvironment in the tumor and cancer cell movement was observed directly via time-lapse fluorescence microscopy over 6 hours. Loss of CaMKK2 significantly hindered cellular movement in both CaMKK2-KO clones when cultured in fresh human adipocytes (**Fig. 2K**; Supplementary Videos S1–S4). To determine the extent to which CaMKK2 is necessary to maintain cancer cell migration *in vitro*, we stably overexpressed this protein in two CaMKK2-KO clones, KK2-KO #1, and KK2-KO #2 (**Fig. 2L**). Overexpression of CaMKK2 rescued the impaired migratory capacity in both knockout clones (**Fig. 2M** and **N**). We conclude that sustained CaMKK2 expression is required to maintain the migratory phenotype of TNBC.

CaMKK2 deficiency impairs metastatic outgrowth from primary tumors *in vivo*

We performed a pilot study to explore the extent to which CaMKK2 depletion impacted metastatic outgrowth from primary tumors. To this end, three CaMKK2 KO clones of luciferase-labeled MDA-MB-231-4175 cells (KK2-KO #1, KK2-KO #2, and KK2-KO #3) and three nonspecific control cell variants (Ctrl #1, Ctrl #3, and Ctrl #5) were orthotopically grafted into the mammary fat pad of immunodeficient mice. The primary tumors were allowed to grow until they reached a size of approximately 2,000 mm^3, following which, the secondary organs were excised and the extent of metastasis was assessed using *ex vivo* bioluminescence imaging (Supplementary Fig. S2A). We observed that CaMKK2 deficiency significantly decreased metastasis of MDA-MB-231-4175 cells to secondary organs (Supplementary Fig. S2B—S2D) and dramatically reduced overall metastatic burden in all three groups bearing CaMKK2-KO tumors (Supplementary Fig. S2E). In contrast, no consistent effect on primary tumor growth was observed when CaMKK2 was depleted (Supplementary Fig. S2F). This indicates that, rather than controlling primary tumor growth, CaMKK2 likely impacts breast tumor pathobiology by controlling metastatic dissemination from the primary tumor.

Metastasis is the endpoint of a series of sequential cell-biological events, starting with the initial migration of tumor cells from the primary site, invasion into the surrounding adipose tissue, resulting ultimately in vascular access (43). The latter steps of the metastatic cascade include extravasation into secondary organs where the disseminated tumor cells that survive may seed the growth of secondary tumors in a metastasis-receptive niche (5, 43). Having established that intratumoral ablation of CaMKK2 impairs spontaneous metastasis, we next determined at which point this enzyme impacts the metastatic cascade. For this study, CaMKK2-KO cells were directly introduced into immunocompromised mice via intravenous injection bypassing the initial steps of the metastatic cascade. Intriguingly, depletion of CaMKK2 in cells directly injected into the circulation had no significant impact on the rate of metastatic outgrowth (Supplementary Fig. S2G and S2H). These data suggest CaMKK2 expression likely impacts overall metastatic progression by positively influencing the initial stages of metastasis, including local migration/invasion of tumor cells from the primary site into the tumor-associated stroma.

To confirm that sustained CaMKK2 expression is necessary for spontaneous metastasis from the primary tumor, we orthotopically grafted CaMKK2-KO cells having stable reexpression of the protein (KO #1-KK2 and KO #2-KK2) into the mammary fat pad of immunocompromised mice. We found that overexpression of CaMKK2 in both knockout clones was accompanied by increased spontaneous metastatic outgrowth in secondary organs and increased total metastatic burden (**Fig. 3A—D**). Interestingly, animals bearing tumors in which CaMKK2 was reexpressed exhibited increased tumor burden when compared with animals bearing CaMKK2-depleted tumors, suggesting that expression of CaMKK2 over and above endogenous levels may alter the biology of primary tumors (Supplementary Fig. S2I). Consistent with the results obtained using genetic approaches, we demonstrated that CaMKK2 inhibitors (STO-609 or GSKi) had no impact on primary tumor growth (**Fig. 4A**), but significantly reduced spontaneous metastasis from the primary tumor (**Fig. 4B–D**). We validated our findings in a second xenograft model of TNBC. Specifically, murine 4T1 cells were orthotopically grafted into the mammary fat pads of immunodeficient mice and it was observed that, while inhibition of CaMKK2 activity had no impact on primary tumor growth (**Fig. 4E**), it significantly reduced spontaneous lung metastasis from the primary tumor (**Fig. 4F**). These findings indicate that CaMKK2 is a targetable regulator of metastatic progression.

Ablation of CaMKK2 disrupts cytoskeletal assembly and cancer cell motility through enhanced phosphorylation of VASP

A characteristic of migrating cells is the presence of intracellular filamentous actin structures (stress fibers), which generate the traction forces necessary to propel cells forward (35). Actin-based stress fibers can be divided into three main groups: "dorsal stress fibers" are thick noncontractile actin filament bundles that elongate radially from the leading edge of migrating cells towards the cell center through vasodilator-stimulated phosphoprotein (VASP)–driven actin polymerization at focal adhesions, "transverse arcs" are thin actin filament bundles that undergo retrograde flow in parallel orientation to the leading edge towards the cell center to ultimately fuse to form thick contractile "ventral stress fibers" that drive tail retraction and cell shape changes in migrating cells (44). While dorsal stress fibers drive directional migration (35), ventral stress fibers are the major force-generating actin structures in migrating cells (45). Given the impact of CaMKK2 inhibition on cell migration and motility, we proceeded to examine whether depletion of CaMKK2 in MDA-MB-231-4175 cells resulted in changes in actin polymerization and stress fiber assembly within these cells. Visualization of F-actin by fluorescent phalloidin staining revealed an almost complete loss of thick dorsal and ventral stress fibers in the CaMKK2-KO cells compared with control cells (**Fig. 5A**; Supplementary Fig. S3). This finding is like that of a previous study that demonstrated in osteosarcoma cells that knockdown of CaMKK2 expression or STO-609-mediated inhibition of CaMKK2 activity resulted in defective actin stress fiber assembly (34). Interestingly, the abnormal stress fiber phenotype in CaMKK2-depleted MDA-MB-231-4175 cells was accompanied by a concomitant increase in the phosphorylation of VASP (**Fig. 5B**). VASP promotes F-actin polymerization by localizing to regions of dynamic actin remodeling to drive actin stress fiber assembly and migration at the leading edge of the cell (46, 47). This protein is a downstream substrate of cAMP-dependent and cGMP-dependent protein kinases (PKA and PKG), which directly phosphorylate VASP at Serine 157 (S157) and Serine 239 (S239), respectively (48, 49). S239 is adjacent to the VASP G-actin binding site (residues 234–237; ref. 50), and its phosphorylation

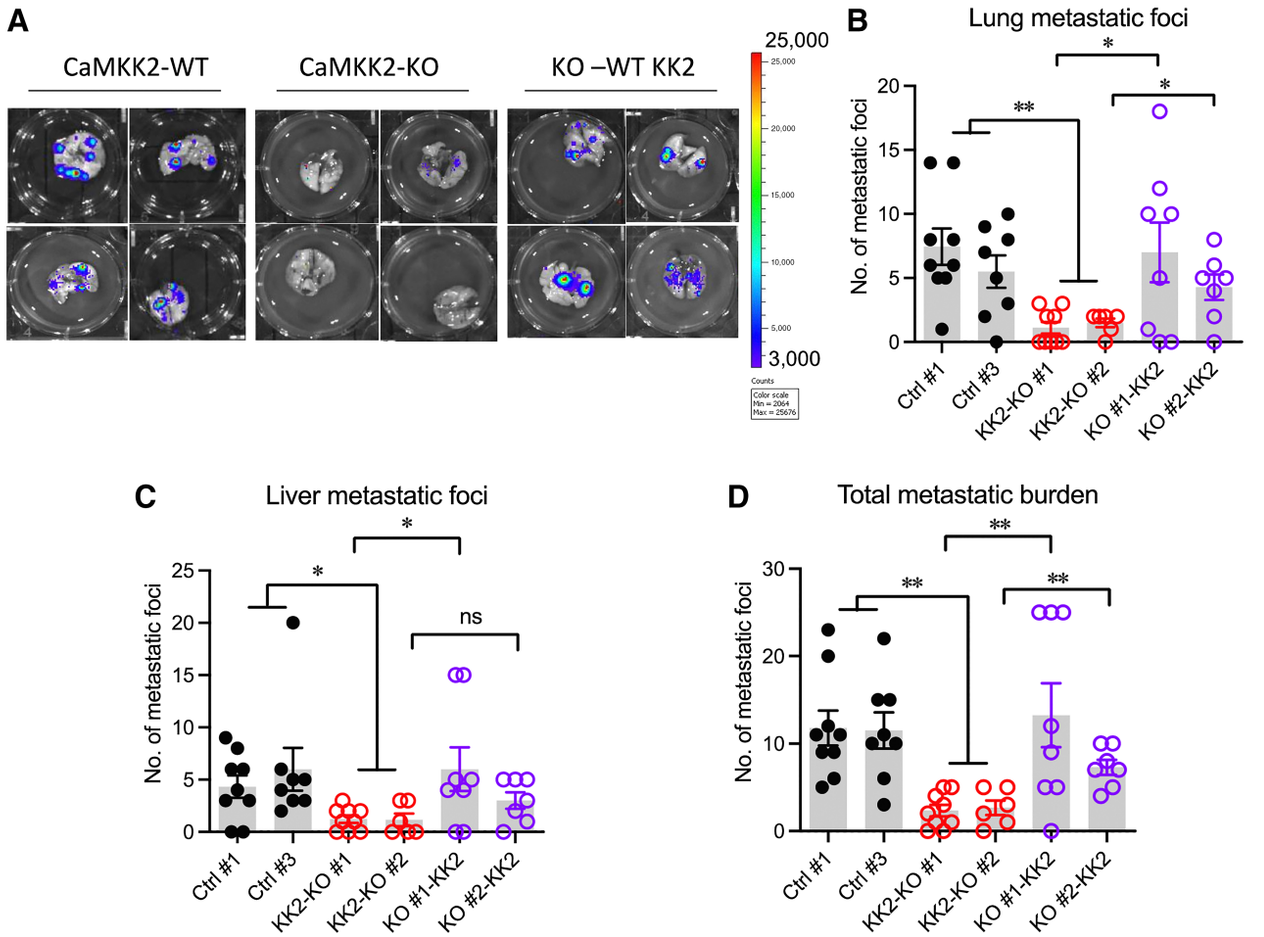

Figure 3.

Genetic ablation of CaMKK2 impairs metastasis from the primary tumor *in vivo*. **A,** Six-week-old female nude mice were orthotopically injected in the mammary fat pad with two control cell clones, Ctrl #1 ($n = 9$), Ctrl #3 ($n = 8$); two CaMKK2-KO cell clones, KK2-KO #1 ($n = 9$), KK2-KO #2 ($n = 6$); and the CaMKK2 KO cell clones with reexpression of CaMKK2, KO #1-KK2 ($n = 8$) and KO #2-KK2 ($n = 7$). All clones were derived from the parental MDA-MB-231–4175 cell line. The mice were sacrificed after tumors reached approximately 2,500 mm^3, and the lung and liver metastatic burden was analyzed *ex vivo*. Representative BLI images showing lung metastatic foci were visualized. **B–D,** Quantitation of the number of metastatic foci in the lung (**B**) and liver (**C**), and total metastatic burden (includes metastatic foci in the liver and lung taken together for each animal; **D**). Data, mean ± SEM. *, $P < 0.05$; **, $P < 0.01$; ns, nonsignificant; by Student *t* test.

inhibits its ability to bind actin and interferes with actin polymerization (51). Notably, PKG preferentially phosphorylates VASP at the S239 site, but subsequently exhibits some residual activity at the S157 residue (48). We observed markedly increased levels of VASP phosphorylation at S239 in CaMKK2-depleted cells that was reinforced by the treatment of cells with a calcium-specific ionophore, ionomycin (**Fig. 5C**). CaMKK2 depletion had a lesser impact on S157 phosphorylation, while S239 was highly phosphorylated in CaMKK2-deficient cells, compared to the controls. Of note, ionomycin-induced Ca^{2+} uptake in control cells did not result in the activation of AMPK (a biomarker for CaMKK2 activity), suggesting that in this context the responses to CaMKK2 activation occurred independently of calcium in MDA-MB-231-4175 cells. Pharmacologic inhibition of CaMKK2 activity also increased phosphorylation of VASP at S239 in both MBA-MB-231 (**Fig. 5D**) and BT-20 cells (**Fig. 5E**). The increase in VASP phosphorylation, in response to CaMKK2 inhibition, tracked with reduced migration with or without ionomycin-induced Ca^{2+} influx in MDA-MB-231-4175 cells (**Fig. 5F**). Similar observations were made in BT-20 cells (**Fig. 5G**). Together, these data suggest that inhibition of CaMKK2 results in increased phosphorylation of VASP to disrupt stress fiber assembly and inhibit TNBC cell motility.

Inhibition of PKG1 restores the migratory capability of CaMKK2-deficient cells

The molecular mechanism(s) by which CaMKK2 regulates VASP phosphorylation was next assessed. Considering that PKG1 is the only upstream kinase that phosphorylates VASP at S239, we hypothesized that its increased activity in CaMKK2-depleted cells may be responsible for the inhibitory phosphorylation of VASP (**Fig. 6A**). To explore this possibility, we assessed the effects of targeting PKG1 activity in CaMKK2-deficient cells using a highly specific, substrate competitive small-molecule inhibitor of this enzyme (RKRARKE; ref. 52). We demonstrated that inhibition of PKG1 activity reduced VASP phosphorylation levels in TNBC cells in which CaMKK2 was inhibited pharmacologically (**Fig. 6B** and **C**) or genetically (**Fig. 6D** and **E**). The ability of RKRARKE to reverse the impact of CaMKK2 inhibition/

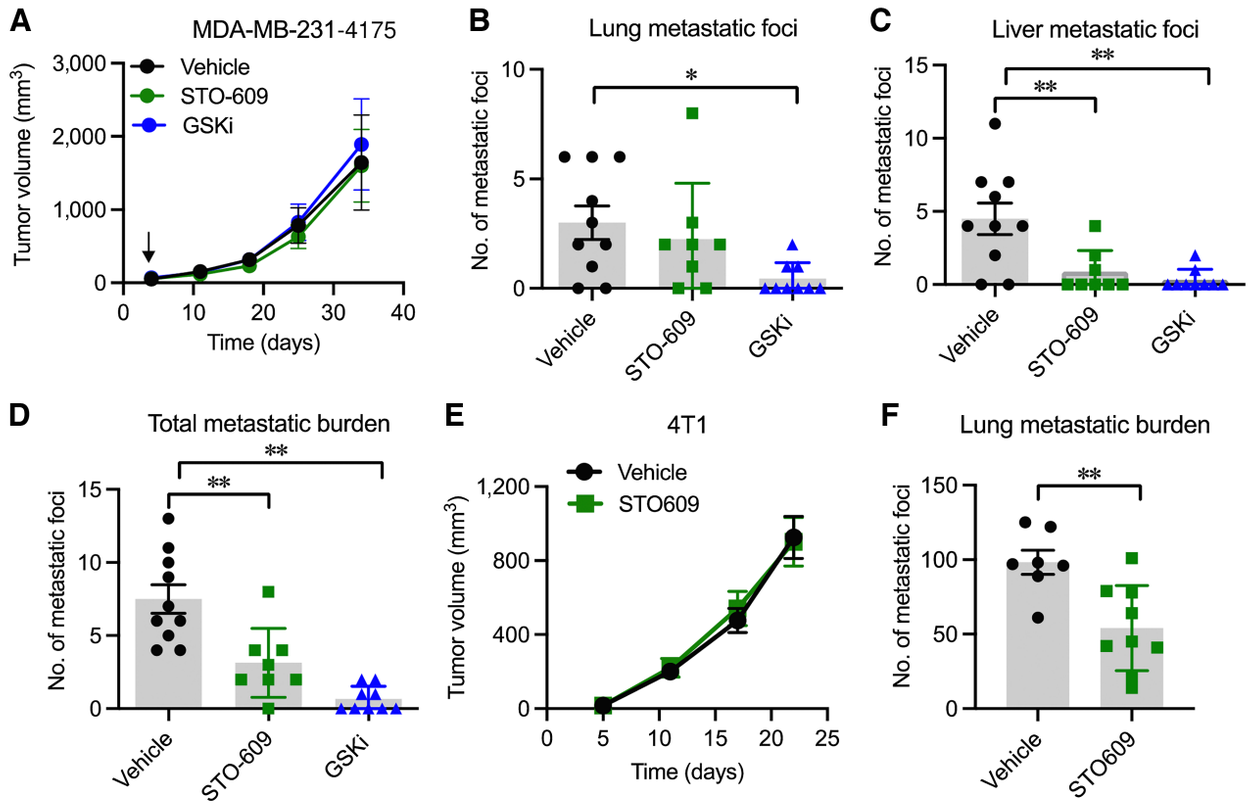

Figure 4.

Pharmacologic inhibition of CaMKK2 impairs metastasis from the primary tumor *in vivo*. **A,** MDA-MB-231-4175 cells were orthotopically injected into the mammary fat pad of 6-week-old female nude mice. Five days postinjection, the animals were dosed with vehicle ($n = 10$), STO-609 (30 mg/kg; $n = 8$), or GSKi (10 mg/kg; $n = 9$) by intraperitoneal injections every third day. Tumor growth rate was monitored until the tumors reached a volume of 2,000 mm^3. **B–D,** Quantitative analysis of metastatic foci in the lung (**B**), liver (**C**), and the total metastatic burden (includes metastatic foci in the liver and lung taken together; **D**). The mice were sacrificed after the primary tumor reached approximately 2000 mm^3, and the metastatic foci were analyzed *ex vivo*. **E,** Subcutaneous tumor growth in 6-week-old female nude mice orthotopically injected with murine 4T1 cells. The mice were randomized (five days after tumor cell injection in the mammary fat pad) and dosed with vehicle ($n = 7$) or STO-609 (30 mg/kg; $n = 9$) by intraperitoneal injections every third day. Tumor growth rate was monitored until the tumors reached a volume of 2,000 mm^3. **F,** Quantitative analysis of metastatic nodules in the lung. Data, mean ± SEM. *, $P < 0.05$; **, $P < 0.01$; by two-way ANOVA followed by Bonferroni multiple-correction test (**A** and **E**) or unpaired Student *t* test (**B–D** and **F**).

depletion on VASP phosphorylation implicated PKG1 as the link between CaMKK2 and cell motility. This was confirmed by showing that pretreatment of cells with RKRARKE restored the migratory phenotype of CaMKK2-KO cells to that of wild-type cells (**Fig. 6F**) and rescued the migration noted in STO-609–treated MDA-MB-231–4175 cells (**Fig. 6G**). Similar results were found using KT5823, an allosteric inhibitor of PKG1 (**Fig. 6H** and **I**; ref. 53). Collectively, these suggest that decreased expression/activity of CaMKK2 in breast cancer cells results in increased PKG1 activity, and that this increases VASP phosphorylation to inhibit stress fiber assembly, ultimately impairing cellular motility and migratory capability.

CaMKK2 indirectly regulates PKG1 activity

It has been established that cGMP is the primary positive regulator of PKG1 activity and thus we posited that CaMKK2 may regulate pathways/processes that control the cellular pool of this second messenger. To this end, we evaluated whether the expression or activity of specific 3′,5′-cyclic nucleotide phosphodiesterases (PDE), which hydrolyze cGMP, modulates PKG1 activity and downstream VASP phosphorylation in metastatic breast cancer cells. The human PDEs comprise a superfamily of 11 enzymes that hydrolyze either cAMP or cGMP. We focused on the PDEs that specifically hydrolyze cGMP (PDE5, PDE6, and PDE9) or that prefer cGMP over cAMP as a substrate (PDE1, PDE3, and PDE10; refs. 54, 55). Intriguingly, CaMKK2 depletion resulted in a quantitative decrease in PDE1A protein levels, while not effecting other PDEs, in all three CaMKK2-KO clones of MDA-MB-231–4175 cells (**Fig. 7A**; Supplementary Fig. S4A). Of the three PDE1 isozymes, PDE1A has the highest affinity for cGMP, with a much lower K_m for cGMP (5 μmol/L) than for cAMP (112 μmol/L; ref. 56). Inhibition of CaMKK2 activity resulted in a similar reduction in PDE1A expression in both MDA-MB-231-4175 cells and BT-20 cells (**Fig. 7B** and **C**). Evaluation of the impact of CaMMK2 on *PDE1A* mRNA expression suggested that this regulatory activity was manifest at the level of transcription (Supplementary Fig. S4B). Interestingly, we found that much like CaMKK2, higher expression of PDE1A is significantly correlated with reduced overall survival in patients with the basal subtype of breast tumors (Supplementary Fig. S4C) but not in patients with luminal or $HER2^+$ disease (Supplementary Fig. S4D–S4F). Indeed, in patients with luminal disease, high PDE1A expression is significantly correlated with increased overall survival, indicating that PDE1A expression may lead to different survival outcomes in patients with luminal disease

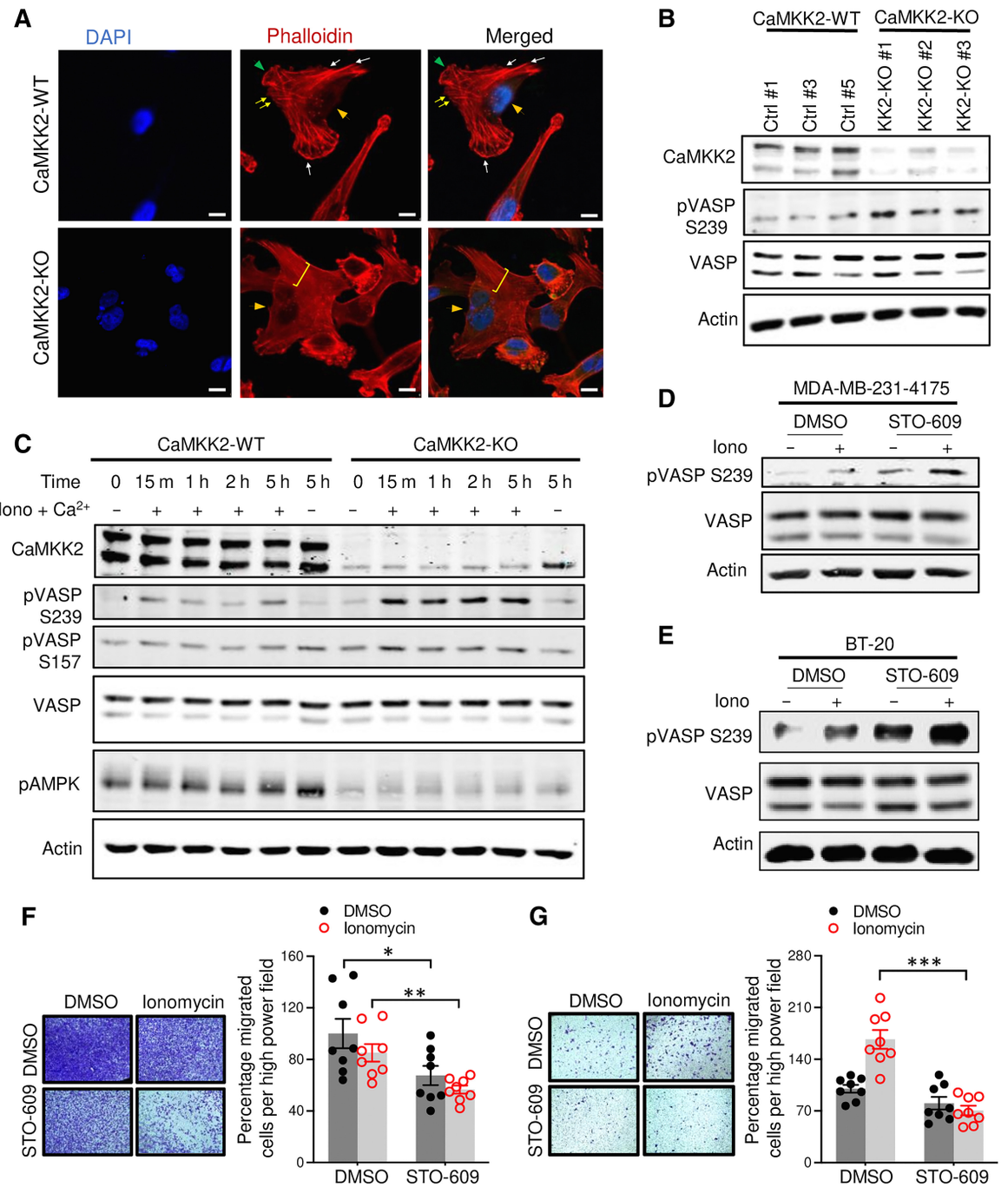

Figure 5.

Depletion of CaMKK2 leads to increased phosphorylation of VASP at the Serine 239 residue, which leads to impaired cytoskeletal assembly and cell motility. **A,** Representative images showing impaired cytoskeletal assembly in CaMKK2-KO cells. Visualization of F-actin by phalloidin staining in CaMKK2-WT (Ctrl #1) and CaMKK2-KO (KK2-KO #1) cells revealed almost complete loss of ventral stress fibers in cells lacking CaMKK2 expression. Yellow arrows, dorsal stress fibers; white arrows, ventral stress fibers; yellow bracket, transverse arcs; green arrowhead, leading edge; yellow arrowhead, contractile rear of the cell. Scale bar, 10 μm. **B,** Representative blot showing increased phosphorylation of VASP at Serine 239 in CaMMK2 KO cell clones. **C,** Representative blot showing VASP phosphorylation at Serine 239 is enhanced in CaMKK2-KO cells in response to ionomycin (1 μmol). Cells were treated with either DMSO or ionomycin (1 μmol/L) with $CaCL_2$ (1 mmol/L) for varying time periods (as indicated). **D** and **E,** Inhibition of CaMKK2 (STO-609, 10 μmol) increases phosphorylation of VASP [especially with ionomycin (1 μmol; 2 hours)] in metastatic MDA-MB-231-4175 cells (**D**) and BT-20 cells (**E**). DMSO or STO-609–treated cells were exposed to either DMSO or ionomycin (1 μmol/L) with $CaCL_2$ (1 mmol/L) for 2 hours before immunoblotting. **F** and **G,** CaMKK2 inhibition decreases migration of MDA-MB-231-4175 cells (**F**) and BT20 cells (**G**) *in vitro*. DMSO or STO-609–treated cells were exposed to either DMSO or ionomycin with $CaCL_2$ (see **D** and **E**) before migration assays were performed. Data are plotted as mean ± SEM; $n = 4$–5 random fields measurements from four individual experiments done in duplicate. *, $P < 0.05$; **, $P < 0.01$; ***, $P < 0.001$. *P* values were calculated using unpaired Student *t* test.

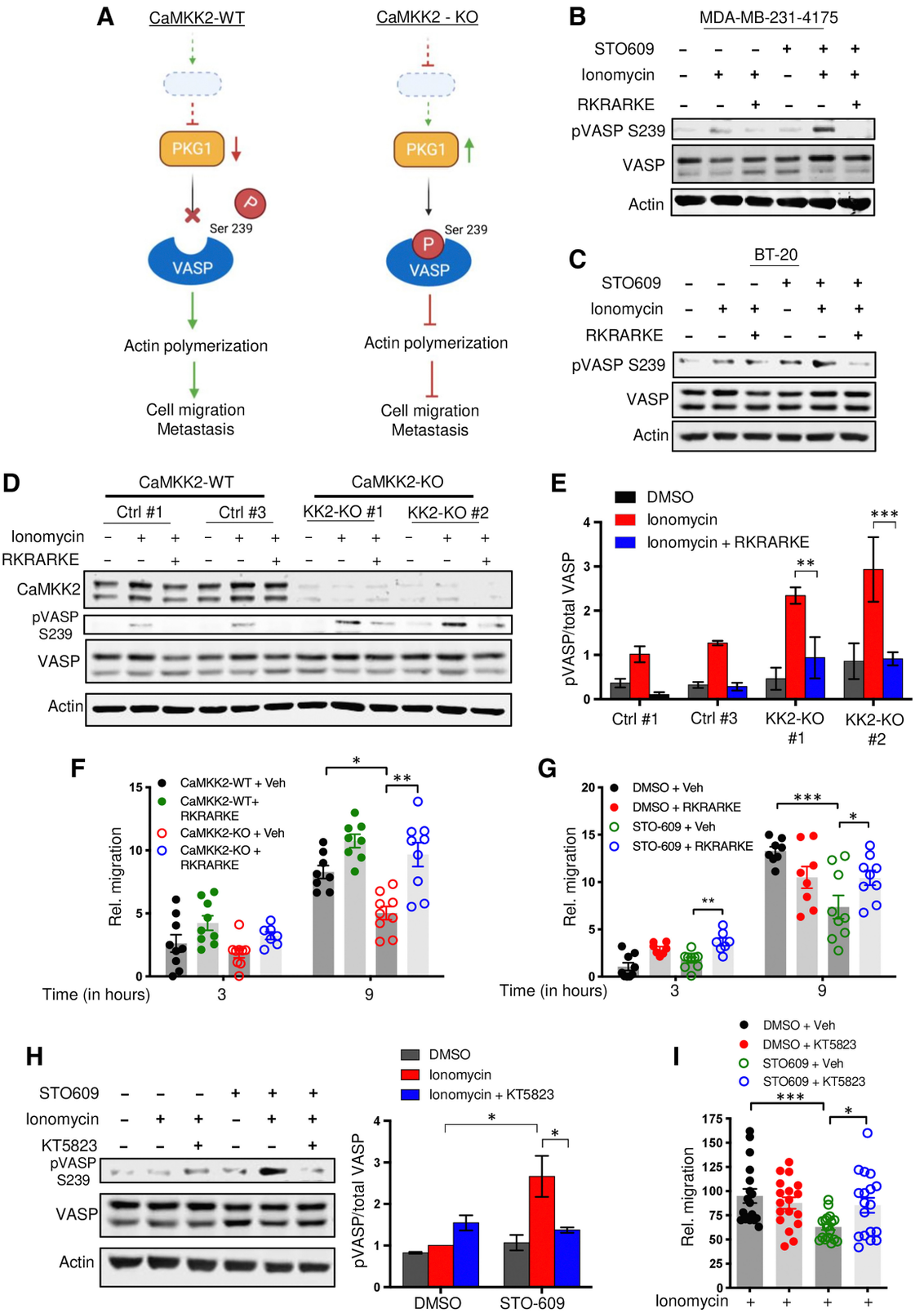
A
CaMKK2-WT
CaMKK2 - KO
PKG1
PKG1
Ser 239
Ser 239
VASP
VASP
Actin polymerization
Actin polymerization
Cell migration
Metastasis
Cell migration
Metastasis
B
MDA-MB-231-4175
STO609
Ionomycin
RKRARKE
pVASP S239
VASP
Actin
C
BT-20
STO609
Ionomycin
RKRARKE
pVASP S239
VASP
Actin
D
CaMKK2-WT
CaMKK2-KO
Ctrl #1
Ctrl #3
KK2-KO #1
KK2-KO #2
Ionomycin
RKRARKE
CaMKK2
pVASP S239
VASP
Actin
E
DMSO
Ionomycin
Ionomycin + RKRARKE
pVASP/total VASP
Ctrl #1
Ctrl #3
KK2-KO #1
KK2-KO #2
F
CaMKK2-WT + Veh
CaMKK2-WT+ RKRARKE
CaMKK2-KO + Veh
CaMKK2-KO + RKRARKE
Rel. migration
Time (in hours)
G
DMSO + Veh
DMSO + RKRARKE
STO-609 + Veh
STO-609 + RKRARKE
Rel. migration
Time (in hours)
H
STO609
Ionomycin
KT5823
pVASP S239
VASP
Actin
DMSO
Ionomycin
Ionomycin + KT5823
pVASP/total VASP
DMSO
STO-609
I
DMSO + Veh
DMSO + KT5823
STO609 + Veh
STO609 + KT5823
Rel. migration
Ionomycin

compared to those with the basal subtype of the disease. Considering that depletion of CaMKK2 reduced PDE1A levels in TNBC cells, we postulated that CaMKK2 may inhibit PKG1 activity and phosphorylation of VASP by driving the expression of PDE1A and decreasing cGMP. We utilized vinpocetine, a PDE1-specific inhibitor (57), IBMx, a pan-PDE inhibitor (58), and sildenafil, a PDE5-specific inhibitor (59) to test this hypothesis. While neither IBMx nor sildenafil increased VASP phosphorylation, the PDE1-specific inhibitor, vinpocetine, increased S239 phosphorylation of VASP in parental MDA-MB-231-4175 cells, phenocopying that which occurred in CaMKK2-depleted/inhibited cells (**Fig. 7D**). Furthermore, inhibition of PDE1 increased the phosphorylation of VASP in CaMKK2-WT cells exposed to ionomycin and did not change the VASP phosphorylation levels in CaMKK2-KO cells (**Fig. 7E**). Inhibition of PDE1 with vinpocetine also reduced the migratory capacity of parental MDA-MB-231-4175 (**Fig. 7F**; Supplementary Fig. S4G) and BT-20 cells (Supplementary Fig. S4H). Of note, siRNA-dependent knockdown of PDE1A expression in parental MDA-MB-231-4175 cells markedly increased VASP phosphorylation at S239 in the presence of ionomycin (Supplementary Fig. S4I), and this increase in VASP phosphorylation tracked with reduced migratory capacity (Supplementary Fig. S4J), phenocopying that which occurred in vinpocetine-treated cells. Finally, we stably overexpressed PDE1A in the CaMKK2-KO clones, KK2-KO #1, and KK2-KO #2. Overexpression of PDE1A in the CaMKK2-KO cells reduced VASP phosphorylation at S239 in the presence of ionomycin (Supplementary Fig. S4K) and rescued the impaired migratory capacity in both knockout clones (Supplementary Fig. S4L and S4M). Together, our data indicate that PDE1A is a critical downstream mediator of CaMKK2-driven cellular migration and motility.

Ionomycin-induced Ca^{2+} influx increased the inhibitory phosphorylation of VASP at S239. This was unrelated to effects on CaMKK2 as it also occurred in CaMKK2-depleted cells. Thus, we sought to understand how elevated calcium increased VASP phosphorylation secondary to activation of the cGMP/PKG1 axis. We hypothesized that this may relate to increased activity of soluble guanylyl cyclase (sGC), which synthesizes cGMP in response to increases in nitrous oxide (NO). This signaling molecule is synthesized by either of three nitric oxide synthases (NOS; NOS-1, NOS-2, and NOS-3). NOS-1 (neuronal NOS) and NOS-3 (endothelial NOS) are constitutively expressed in most cells and require Ca^{2+} for activity, while NOS-2 (inducible NOS) activity is triggered by inflammatory stimuli, independent of Ca^{2+} influx (60, 61). Thus, we postulated that increased Ca^{2+} influx activates NOS-1 or NOS-3 (or both), thereby inducing cGMP production. Indeed, N_{ω}-Nitro-L-arginine (L-NNA), a competitive inhibitor of NOS-1 and NOS-3, blocked ionomycin-induced VASP phosphorylation in both CaMKK2-KO and control cells (**Fig. 7G** and **H**). This indicates that intracellular Ca^{2+} plays a key role in driving PKG1 activation/VASP phosphorylation by increasing cGMP production through the activation of NOS-1 and NOS-3. However, this effect is counteracted by CaMKK2/PDE1 activity to ultimately restrict aberrant PKG1 activity and downstream VASP phosphorylation in migratory cells. Of note, the negative impact of CaMKK2 knockdown on cell migration was reversed by treatment with L-NNA (**Fig. 7I**). Taken together, our results indicate that CaMKK2 is required to maintain PDE1A expression in TNBC cells, which, by hydrolyzing cGMP attenuates PKG1 activity, ultimately support tumor cell migration and spontaneous metastatic progression in breast cancer (**Fig. 7J**).

CaMKK2 expression is associated with poor progression-free survival and higher metastasis in HGSOC

We next addressed whether CaMKK2 expression was elevated and/or its activity associated with increased metastatic capacity in cancers other than those of the breast. HGSOC and TNBC are genetically similar cancers and share many underlying molecular features, such as *BRCA1* and *BRCA2* germline mutations and *TP53* somatic mutations (3). Moreover, we have observed that, much like in TNBC cells, depletion/inhibition of CaMKK2 in ovarian cancer cells impaired their migratory ability *in vitro* (Supplementary Fig. S1D and S1E). We evaluated CaMKK2 expression levels in tumors from 62 patients diagnosed with advanced stage HGSOC, fallopian tube or primary peritoneal cancer and found that higher expression (Intensity score >3; **Fig. 8A**) was directly correlated with worse progression-free survival (PFS; **Fig. 8B**) and overall survival (OS; **Fig. 8C**) in patients with advanced stage (stage III) HGSOC. In a separate study of samples from patients with stage II to IV HGSOC, we found that low expression of CaMKK2 (intensity score <3) was associated with longer PFS (**Fig. 8D**), and a trend toward higher median OS in this expanded cohort was observed (**Fig. 8E**). Our findings suggest that much like in TNBC, higher intratumoral CaMKK2 expression is predictive of highly aggressive phenotypes in patients with advanced stage HGSOC. Importantly, pharmacological inhibition of CaMKK2 in animals injected with SKOV3ip cells, a validated model of HGSOC, significantly diminished spontaneous metastatic outgrowth, compared to vehicle-treated animals (**Fig. 8F** and **G**), indicating that intratumoral CaMKK2 activity may be required to maintain metastatic capacity in HGSOC. From a clinical perspective, patients with HGSOC often present with metastatic disease, especially in the abdominal cavity. Despite standard-of-care cytoreductive surgery to resect tumor burden from any involved organs in the abdominal and pelvic cavity, most

Figure 6.

Inhibition of PKG1 blocks phosphorylation of VASP in CaMKK2-depleted cells and restores cellular migration *in vitro*. **A,** Schematic representation of working hypothesis of the mechanism by which CaMKK2 drives cell migration and metastasis **B** and **C**, RKRARKE treatment (100 μmol; 2.5 hours) decreased VASP phosphorylation in CaMKK2-inhibited MDA-MB-231-4175 cells (**B**) and BT-20 cells (**C**). Vehicle or STO-609–treated cells were dosed with RKRARKE for 30 minutes before exposure to DMSO or ionomycin (1 μmol/L) with $CaCL_2$ (1 mmol/L) for 2 hours. Representative immunoblots from three independent experiments (**B**) and one experiment (**C**) are shown. **D** and **E,** Inhibition of PKG1 with RKRARKE blocks VASP phosphorylation at Serine 239 in CaMKK2-KO cells. CaMKK2-WT (Ctrl #1) and CaMKK2-KO (KK2-KO #1) cells were pretreated with RKRARKE (100 μmol) for 30 minutes before exposure to DMSO or ionomycin (1 μmol/L) with $CaCL_2$ (1 mmol/L) for 2 hours. Representative blots from two independent experiments (**D**) and quantitative results for the band intensities of phospho-VASP versus total VASP (**E**) are shown. **F** and **G,** RKRARKE (100 μmol; 2.5 hours) pretreatment restores the migratory phenotype in CaMKK2-KO cells (**F**) and STO-609-treated MDA-MB-231-4175 cells (**G**). Cells were pretreated with RKRARKE before exposure to ionomycin (1 μmol/L) with $CaCL_2$ (1 mmol/L) for 2 hours prior to migration assays. Data plotted as mean ± SEM; $n = 4$–5 random fields measurements from two individual experiments. **H,** Pretreatment with KT5823 (5 μmol; 16 hours) in CaMKK2-inhibited cells decreased VASP phosphorylation. MDA-MB-231-4175 cells were pretreated with either vehicle or KT5823 overnight before exposure to DMSO or ionomycin. Representative blots (left) and quantitative analysis (right) of band intensities from two independent experiments are shown. **I,** KT5823 pretreatment (5 μmol; 16 hours) of CaMKK2-inhibited cells restores the migratory phenotype of STO-609–treated MDA-MB-231-4175 cells. Data are plotted as mean ± SEM; $n = 4$–5 random fields measurements from four individual transwells. *, $P < 0.05$; **, $P < 0.01$; ***, $P < 0.001$. P values were calculated using unpaired Student t test.

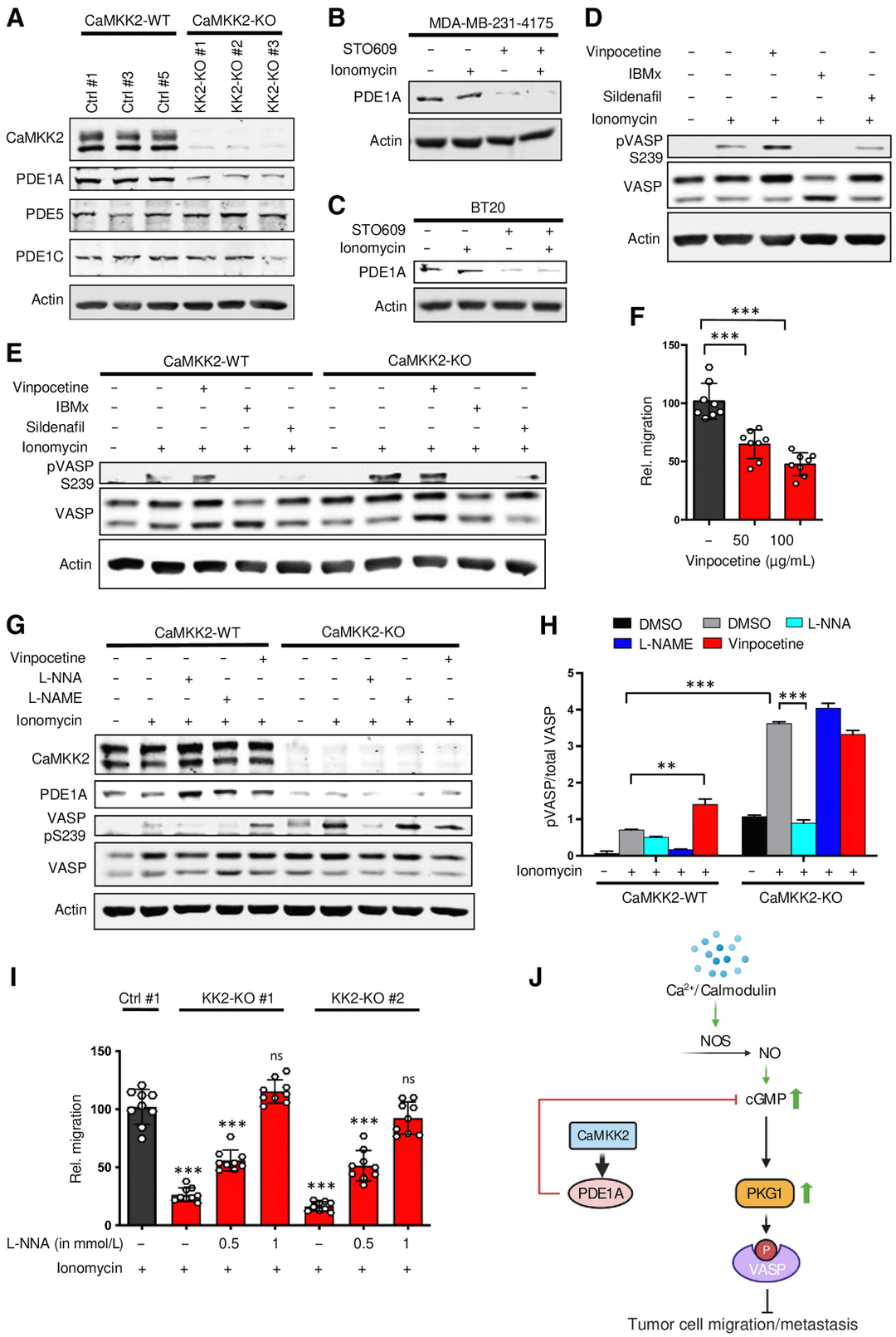
A
CaMKK2-WT
CaMKK2-KO
Ctrl #1
Ctrl #3
Ctrl #5
KK2-KO #1
KK2-KO #2
KK2-KO #3
CaMKK2
PDE1A
PDE5
PDE1C
Actin
B
MDA-MB-231-4175
STO609
Ionomycin
PDE1A
Actin
C
BT20
STO609
Ionomycin
PDE1A
Actin
D
Vinpocetine
IBMx
Sildenafil
Ionomycin
pVASP S239
VASP
Actin
E
CaMKK2-WT
CaMKK2-KO
Vinpocetine
IBMx
Sildenafil
Ionomycin
pVASP S239
VASP
Actin
F
***
***
Rel. migration
150
100
50
0
–
50
100
Vinpocetine (μg/mL)
G
CaMKK2-WT
CaMKK2-KO
Vinpocetine
L-NNA
L-NAME
Ionomycin
CaMKK2
PDE1A
VASP pS239
VASP
Actin
H
DMSO
DMSO
L-NNA
L-NAME
Vinpocetine
pVASP/total VASP
***
***
**
Ionomycin
CaMKK2-WT
CaMKK2-KO
I
Ctrl #1
KK2-KO #1
KK2-KO #2
Rel. migration
150
100
50
0
ns
ns
***
***
***
***
L-NNA (in mmol/L)
Ionomycin
J
Ca2+/Calmodulin
NOS
NO
cGMP
CaMKK2
PDE1A
PKG1
P
VASP
Tumor cell migration/metastasis

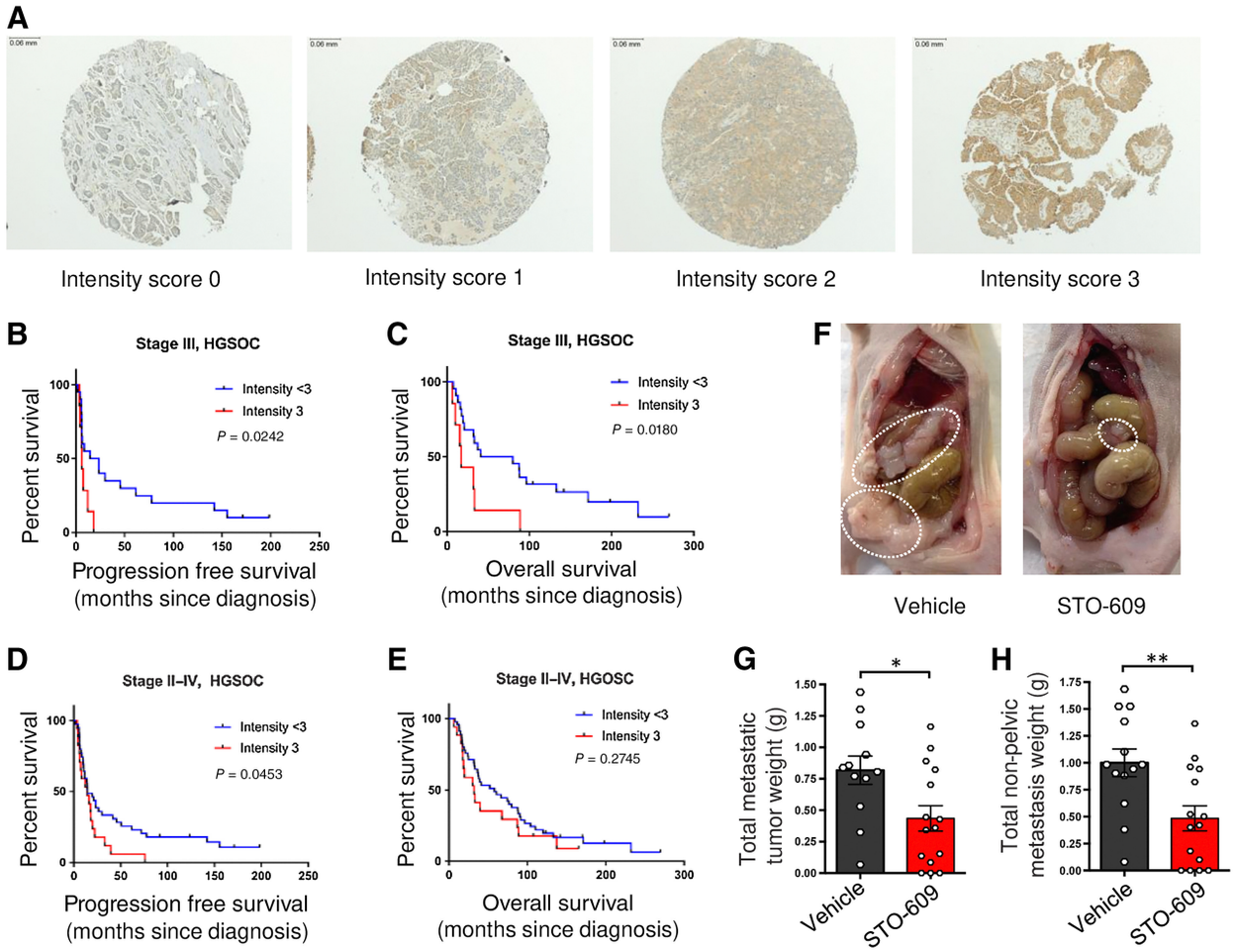

Figure 8.

CaMKK2 expression is associated with lower survival rates in patients with HGSOC. **A,** Representative photomicrographs of tumor microarray sections stained for CaMKK2 by immunohistochemistry, with corresponding intensity scores (×10 magnification). **B** and **C,** PFS (**B**) and OS (**C**) of patients with stage III HGSOC were evaluated and demonstrated that low CaMKK2 expression (intensity score < 3) correlated with longer median PFS (19.1 months vs. 6.2 months, $P = 0.0242$) and OS (60.6 vs. 17.1 months, $P = 0.0180$) than patients with high expression. **D,** PFS of patients with stage II to IV HGSOC were evaluated, which demonstrated that low CaMKK2 expression correlated with longer median PFS than patients with high expression (14.7 months vs. 14.5 months, $P = 0.0453$). **E,** OS of patients with stage II to IV were evaluated and showed a trend toward higher median OS in patients with low expression (58.0 months vs. 32 months, $P = 0.2745$). **F,** Eight-week-old female nude mice were inoculated with SKOV3ip1 cells (intraperitoneally) and received vehicle (control) or STO-609. Representative images (**F**), weight of metastatic tumor burden (**G**), and weight of non-pelvic metastasis (**H**) are shown ($n = 15$ per group). Data, mean ± SEM. *, $P < 0.05$; **, $P < 0.01$; by Student *t* test (**G** and **H**) and log-rank test (**B**–**E**).

Figure 7.

Depletion of CaMKK2 causes reduced expression of PDE1A, an upstream negative regulator of PKG1. **A,** CaMKK2 depletion decreased PDE1A protein levels in MDA-MB-231-4175 cells. **B** and **C,** Inhibition of CaMKK2 (STO-609, 10 μmol/L) reduced PDE1A expression in MDA-MB-231-4175 cells (**B**) and BT20 cells (**C**). **D,** PDE1 inhibition with vinpocetine increased VASP phosphorylation at Serine 239 in MDA-MB-231-4175 cells. Cells were pretreated with vinpocetine (50 μg/mL; 16 hours), IBMx (100 μmol/L; 16 hours), or sildenafil (10 μmol/L; 1 hour) before exposure to either DMSO or ionomycin (1 μmol/L) with $CaCL_2$ (1 mmol/L) for 2 hours **E,** Vinpocetine pretreatment enhances phosphorylation of VASP at Serine 239 in CaMKK2-WT cells, phenocopying CaMKK2-KO cells. **F,** PDE1 inhibition impairs migration of MDA-MB-231-4175 cells in a dose-dependent manner. Following pretreatment with vinpocetine, MDA-MB-231-4175 cells were exposed to ionomycin (1 μmol/L) with $CaCL_2$ (1 mmol/L) for 2 hours before assaying for migration. Data plotted as mean ± SEM; $n = 4$–5 random fields measurements from two individual experiments. **G** and **H,** Treatment with L-NNA blocked VASP phosphorylation in ionomycin-treated CaMKK2-KO cells. CaMKK2-WT and CaMKK2-KO cells were cultured with NOS inhibitors (16 hours) or vinpocetine, as indicated, before exposure to either DMSO or ionomycin (1 μmol/L) with $CaCL_2$ (1 mmol/L) for 2 hours. Representative blots (**G**) and quantitative results (**H**) for the band intensities of phospho-VASP versus total VASP are shown. Data plotted as mean ± SEM from two independent experiments. **I,** Pretreatment of CaMKK2-KO cell lines with L-NNA rescued migratory ability in a dose-dependent manner. CaMKK2-KO cells were cultured with or without L-NNA (1 mmol/L; 16 hours) before exposure to ionomycin (1 μmol/L) with $CaCL_2$ (1 mmol/L) for 2 hours and assayed for migration. Data plotted as mean ± SEM; $n = 4$–5 random fields measurements from two individual experiments. Significance calculated relative to Ctrl#1. **J,** Schematic model of the mechanism by which CaMKK2 drives tumor cell migration and metastasis. **, $P < 0.01$; ***, $P < 0.005$; ns, nonsignificant. *P* values were calculated using unpaired Student *t* test.

HGSOC patients remain at high risk of recurrence following primary treatment due to secondary metastasis beyond the abdominal cavity. It was significant, therefore, that in addition to impacting overall metastatic burden, inhibition of CaMKK2 activity significantly reduced invasive metastatic outgrowth in secondary sites, distant from the abdominal and pelvic cavity (**Fig. 8H**). Our results suggest that targeting CaMKK2 may be an effective therapeutic approach to limit secondary relapse in HGSOC.

Discussion

The development of metastasis requires tumor cells to dissociate from their primary site, acquire migratory capability and invade the basement membrane and surrounding tissue to ultimately gain vascular access (62). Only a small percentage of cells that are shed from the primary tumor possess these invasive (and metastasis-initiating) properties. Here, we show that tumor cell intrinsic expression of CaMKK2 is a key determinant of the metastatic potential of TNBC cells. Specifically, genetic ablation of CaMKK2, or its pharmacological inhibition, dramatically reduced the invasiveness and migratory potential of cell lines modeling TNBC *in vitro* and significantly reduced spontaneous metastatic outgrowth from primary tumors *in vivo*. Importantly, sustained CaMKK2 activity was found to be required to maintain metastatic capacity in HGSOC, a high-risk, poor prognosis ovarian cancer subtype that shares many genetic features with TNBC. Mechanistically, our results implicate an intricate signaling axis in which CaMKK2 plays a central role in controlling intracellular actin dynamics to favor heightened tumor cell motility and migratory capability. We find that CaMKK2 restricts PKG1 activity in metastatic tumor cells by driving the expression of PDE1A, a key phosphodiesterase that catalyzes the degradation of intracellular cGMP. This implicates CaMKK2 as a key driver of the negative regulatory mechanism that counteracts NOS-mediated cGMP synthesis to ultimately maintain low levels of PKG1 activation and limit the inhibitory phosphorylation of VASP in metastatic tumor cells. Loss of CaMKK2 shifts the balance towards increased intracellular cGMP production, leading to enhanced PKG1 activation and increased phosphorylation of VASP. This inhibitory phosphorylation event impairs VASP-driven actin polymerization and stress fiber assembly to ultimately impact tumor cell motility and metastatic capability in TNBC.

Consistent with our findings, higher expression of CaMKK2 or PDE1A was associated with reduced overall survival in patients with the basal subtype of breast tumors. Interestingly, high PDE1A expression was correlated with increased overall survival in patients with luminal disease. Considering that the expression of CaMKK2 is low in tumors of the luminal subtype (33), we believe that the effect of PDE1A expression on the pathobiology of luminal disease may be largely independent of the upstream regulatory effects of CaMKK2. Thus, increased PDE1A levels may affect the progression of tumors of the luminal subtype through a pathway distinct from the CaMKK2–PDE1A–VASP signaling mechanism that we identified in this study, thereby leading to different survival outcomes in patients with luminal disease compared to those with the basal subtype of breast tumors.

Although CaMKK2 has been demonstrated to have distinct protumorigenic roles in several cancers (30, 32, 63), the mechanisms by which it impacts tumor metastasis have not been elucidated. A cell-based study implicated CaMKK2 activity in medulloblastoma migration (64), and we previously reported that CaMKK2 inhibition impaired androgen-dependent invasion/migration of prostate cancer cells *in vitro* (29). More recently, CaMKK2 activity was shown to decrease anoikis, thereby aiding metastatic progression in lung cancer (25). These observations, and our new data showing that elevated CaMKK2 expression is associated with aggressive disease phenotypes in both TNBC and HGSOC, highlight the importance of this enzyme in tumor pathobiology and suggest that it may be a useful therapeutic target for the clinical management of several different tumor types.

VASP is a substrate of cGMP-dependent protein kinases (PKA and PKG), which localizes to regions of dynamic actin remodeling to promote F-actin assembly where it integrates signaling events that regulate cytoskeletal reorganization and cell movement (46, 51, 65). Originally, VASP phosphorylation was described in platelets, where both PKA and PKG were shown to phosphorylate Serine 157 and Serine 239, respectively (66). Notably, the S239 site is adjacent to the VASP G-actin binding site and phosphorylation at this residue inhibits its ability to bind actin causing a significant reduction in VASP-driven F-actin accumulation (51). Our results indicate that sustained CaMKK2 expression drives tumor cell motility by negatively regulating PKG1 activity in migratory cells, thereby limiting the inhibitory phosphorylation of VASP at the S239 site. Apart from facilitating stress fiber assembly within migratory cells, VASP-dependent actin polymerization is crucial for the formation of actin-containing protrusions (filopodia and lamellipodia) and invadopodia that enable cells to invade through the basement membrane (67, 68). Future studies will explore the direct connections between CaMKK2, VASP, and the formation of these specialized structures.

The NO/cGMP/PKG1 pathway is involved in the regulation of several cellular processes and is tightly regulated by phosphodiesterase-dependent hydrolysis of cGMP (54). It is significant, therefore, that CaMKK2 was found to be an upstream regulator of *PDE1A* mRNA and protein expression and that depletion of CaMKK2 induced the activity of PKG1, a major downstream effector of the NO/cGMP signaling axis. Notably, VASP is a primary downstream substrate for PKG1 and the phosphorylation of this protein at the S239 site is used as a readout for PKG1 activity (69, 70). Our data suggest that VASP is the primary biochemical link between PKG1 and increased cell motility/metastasis. Recently, it has been shown that PKG1 can also phosphorylate TSC2 to inhibit mTORC1 signaling although the role of this activity in metastasis has not been explored (71).

The somatic molecular profiles of TNBC and HGSOC share many similarities, including frequent *TP53* mutations, inactivation of *BRCA1* and *BRCA2* and overall poor prognosis (3, 9). Patients with HGSOC often present with metastatic disease, especially in the pelvic and abdominal cavity. Given that the five-year overall survival for patients with Stage III and IV disease remains approximately 20% to 40% (12), improving upon the current standard of care in HGSOC represents a critical unmet need. Our data, which demonstrated a very strong protective effect of CaMKK2 inhibitors in animal models of advanced ovarian cancer, highlight a potential role for these drugs in the long-term management of HGSOG by preventing/decreasing metastatic progression of postoperative residual disease. Similarly, TNBC is the most aggressive subtype of breast cancer, and these tumors tend to become highly invasive early during cancer development. Recent data have suggested that isolated local or regional relapses (ILRR), defined as clinically documented relapse in the ipsilateral breast or regional nodes within one year of the primary diagnosis, significantly increased the risk of distant recurrence and death in breast cancer patients (72). This suggests that patients with TNBC patients present with lymph node–positive, early-stage disease or develop local relapses within a year of first-line treatment may benefit from neoadjuvant combination therapies targeting CaMKK2 in conjunction with standard chemotherapy.

The immune checkpoint inhibitor pembrolizumab [anti-programmed cell death protein-1 (PD-1) monoclonal antibody] was recently approved for use in high-risk, early-stage TNBC, in combination with neoadjuvant chemotherapy and as a single agent in the adjuvant setting postsurgery (73). Furthermore, there are ongoing clinical trials evaluating the effectiveness of pembrolizumab in platinum-resistant advanced ovarian cancer (ClinicalTrials.gov Identifier: NCT02440425). We previously demonstrated that targeting myeloid-specific CaMKK2 in the mammary tumor microenvironment significantly enhances antitumor immune responses by reducing the immunosuppressive activity of tumor-associated macrophages and increasing the recruitment of cytotoxic T cells into the tumor (33). This suggests that CaMKK2 inhibitors may increase the efficacy of immune checkpoint inhibitors in cancers that are enriched in tumor-associated macrophages. The observation in this study that CaMKK2 also regulates the metastatic potential of cancer cells suggests that CaMKK2 inhibitors will have a dual action in tumors and when used with ICBs could significantly advance the pharmacotherapy of breast and ovarian cancers.

Authors' Disclosures

R.A. Previs reports grants from AAOGF-GOG Foundation during the conduct of the study and other support from Labcorp outside the submitted work. K.C. Strickland reports other support from Labcorp during the conduct of the study and personal fees from Almac Pharmaceuticals, Foundation Medicine, Canaria Bio, and OncoQuest Pharmaceuticals outside the submitted work. F.H. Lau reports other support from Keliomics outside the submitted work. C. Chang reports grants from Department of Defense Breast Cancer Research Program and Celgene (BMS) during the conduct of the study. D.P. McDonnell reports grants from Department of Defense, and grants and personal fees from BMS during the conduct of the study and grants, personal fees, and nonfinancial support from Zentalis, Celgene, and RAPPTA Therapeutics, Novartis, G1 Therapeutics, and Radius Health outside the submitted work, as well as a patent for US9,999,620 issued. No disclosures were reported by the other authors.

Authors' Contributions

D. Mukherjee: Conceptualization, data curation, formal analysis, validation, investigation, writing–original draft, writing–review and editing. **R.A. Previs:** Investigation. **C. Haines:** Investigation. **M. Al Abo:** Formal analysis. **P.K. Juras:** Investigation. **K.C. Strickland:** Formal analysis. **B. Chakraborty:** Investigation. **S. Artham:** Investigation. **R.S. Whitaker:** Investigation. **K. Hebert:** Investigation. **J. Fontenot:** Investigation. **S.R. Patierno:** Supervision. **J.A. Freedman:** Supervision. **F.H. Lau:** Supervision, investigation. **M.E. Burow:** Supervision. **C.-Y. Chang:** Conceptualization, supervision, writing–review and editing. **D.P. McDonnell:** Conceptualization, supervision, writing–review and editing.

Acknowledgments

This project was supported by U.S. Department of Defense Award (BC191370) to D.P. McDonnell. R.A. Previs is supported by grants from the NIH 1K12HD103083–01, AAOGF-GOG Foundation, and the Emerson Collective. S.R. Patierno and J.A. Freedman are supported by NIH Basic Research in Cancer Health Disparities R01 Award (R01CA220314).

The publication costs of this article were defrayed in part by the payment of publication fees. Therefore, and solely to indicate this fact, this article is hereby marked "advertisement" in accordance with 18 USC section 1734.

Note

Supplementary data for this article are available at Cancer Research Online (http://cancerres.aacrjournals.org/).

Received May 17, 2022; revised January 5, 2023; accepted June 13, 2023; published first June 19, 2023.

References

1. Sung H, Ferlay J, Siegel RL, Laversanne M, Soerjomataram I, Jemal A, et al. Global cancer statistics 2020: GLOBOCAN estimates of incidence and mortality worldwide for 36 cancers in 185 countries. CA Cancer J Clin 2021;71:209–49.
2. Siegel RL, Miller KD, Jemal A. Cancer statistics, 2017. CA Cancer J Clin 2017;67:7–30.
3. The Cancer Genome Atlas Network. Comprehensive molecular portraits of human breast tumours. Nature 2012;490:61–70.
4. Allemani C, Matsuda T, Di Carlo V, Harewood R, Matz M, Niksic M, et al. Global surveillance of trends in cancer survival 2000–14 (CONCORD-3): analysis of individual records for 37 513 025 patients diagnosed with one of 18 cancers from 322 population-based registries in 71 countries. Lancet 2018;391:1023–75.
5. Valastyan S, Weinberg RA. Tumor metastasis: molecular insights and evolving paradigms. Cell 2011;147:275–92.
6. Li Y, Yang D, Chen P, Yin X, Sun J, Li H, et al. Efficacy and safety of neoadjuvant chemotherapy regimens for triple-negative breast cancer: a network meta-analysis. Aging (Albany NY) 2019;11:6286–311.
7. Liedtke C, Mazouni C, Hess KR, Andre F, Tordai A, Mejia JA, et al. Response to neoadjuvant therapy and long-term survival in patients with triple-negative breast cancer. J Clin Oncol 2008;26:1275–81.
8. von Minckwitz G, Untch M, Blohmer JU, Costa SD, Eidtmann H, Fasching PA, et al. Definition and impact of pathologic complete response on prognosis after neoadjuvant chemotherapy in various intrinsic breast cancer subtypes. J Clin Oncol 2012;30:1796–804.
9. The Cancer Genome Atlas Research Network. Integrated genomic analyses of ovarian carcinoma. Nature 2011;474:609–15.
10. du Bois A, Reuss A, Pujade-Lauraine E, Harter P, Ray-Coquard I, Pfisterer J. Role of surgical outcome as prognostic factor in advanced epithelial ovarian cancer: a combined exploratory analysis of 3 prospectively randomized phase 3 multicenter trials: by the Arbeitsgemeinschaft Gynaekologische Onkologie Studiengruppe Ovarialkarzinom (AGO-OVAR) and the Groupe d'Investigateurs Nationaux Pour les Etudes des Cancers de l'Ovaire (GINECO). Cancer 2009;115:1234–44.
11. Schorge JO, Eisenhauer EE, Chi DS. Current surgical management of ovarian cancer. Hematol Oncol Clin North Am 2012;26:93–109.
12. Heintz AP, Odicino F, Maisonneuve P, Quinn MA, Benedet JL, Creasman WT, et al. Carcinoma of the ovary. FIGO 26th annual report on the results of treatment in gynecological cancer. Int J Gynaecol Obstet 2006;95 Suppl 1:S161–92.
13. Racioppi L, Means AR. Calcium/calmodulin-dependent protein kinase kinase 2: roles in signaling and pathophysiology. J Biol Chem 2012;287:31658–65.
14. Anderson KA, Means RL, Huang QH, Kemp BE, Goldstein EG, Selbert MA, et al. Components of a calmodulin-dependent protein kinase cascade. Molecular cloning, functional characterization and cellular localization of Ca2+/calmodulin-dependent protein kinase kinase beta. J Biol Chem 1998;273:31880–9.
15. Marcelo KL, Means AR, York B. The Ca(2+)/Calmodulin/CaMKK2 axis: nature's metabolic camshaft. Trends Endocrinol Metab 2016;27:706–18.
16. Schmitt JM, Wayman GA, Nozaki N, Soderling TR. Calcium activation of ERK mediated by calmodulin kinase I. J Biol Chem 2004;279:24064–72.
17. Peters M, Mizuno K, Ris L, Angelo M, Godaux E, Giese KP. Loss of Ca2+/calmodulin kinase kinase beta affects the formation of some, but not all, types of hippocampus-dependent long-term memory. J Neurosci 2003;23:9752–60.
18. Cary RL, Waddell S, Racioppi L, Long F, Novack DV, Voor MJ, et al. Inhibition of Ca(2)(+)/calmodulin-dependent protein kinase kinase 2 stimulates osteoblast formation and inhibits osteoclast differentiation. J Bone Miner Res 2013;28:1599–610.
19. Wayman GA, Kaech S, Grant WF, Davare M, Impey S, Tokumitsu H, et al. Regulation of axonal extension and growth cone motility by calmodulin-dependent protein kinase I. J Neurosci 2004;24:3786–94.
20. Lin F, Marcelo KL, Rajapakshe K, Coarfa C, Dean A, Wilganowski N, et al. The camKK2/camKIV relay is an essential regulator of hepatic cancer. Hepatology 2015;62:505–20.

21. Oury F, Yadav VK, Wang Y, Zhou B, Liu XS, Guo XE, et al. CREB mediates brain serotonin regulation of bone mass through its expression in ventromedial hypothalamic neurons. Genes Dev 2010;24:2330–42.
22. Anderson KA, Ribar TJ, Lin F, Noeldner PK, Green MF, Muehlbauer MJ, et al. Hypothalamic CaMKK2 contributes to the regulation of energy balance. Cell Metab 2008;7:377–88.
23. Anderson KA, Lin F, Ribar TJ, Stevens RD, Muehlbauer MJ, Newgard CB, et al. Deletion of CaMKK2 from the liver lowers blood glucose and improves whole-body glucose tolerance in the mouse. Mol Endocrinol 2012;26:281–91.
24. Lin F, Ribar TJ, Means AR. The Ca2+/calmodulin-dependent protein kinase kinase, CaMKK2, inhibits preadipocyte differentiation. Endocrinology 2011;152:3668–79.
25. Jin L, Chun J, Pan C, Kumar A, Zhang G, Ha Y, et al. The PLAG1-GDH1 axis promotes anoikis resistance and tumor metastasis through CamKK2-AMPK signaling in LKB1-deficient lung cancer. Mol Cell 2018;69:87–99.
26. Hall DP, Cost NG, Hegde S, Kellner E, Mikhaylova O, Stratton Y, et al. TRPM3 and miR-204 establish a regulatory circuit that controls oncogenic autophagy in clear cell renal cell carcinoma. Cancer Cell 2014;26:738–53.
27. Vara-Ciruelos D, Dandapani M, Gray A, Egbani EO, Evans AM, Hardie DG. Genotoxic damage activates the AMPK-alpha1 isoform in the nucleus via Ca(2+)/CaMKK2 signaling to enhance tumor cell survival. Mol Cancer Res 2018;16:345–57.
28. Zhang Y, Recouvreux MV, Jung M, Galenkamp KMO, Li Y, Zagnitko O, et al. Macropinocytosis in cancer-associated fibroblasts is dependent on CaMKK2/ARHGEF2 signaling and functions to support tumor and stromal cell fitness. Cancer Discov 2021;11:1808–25.
29. Frigo DE, Howe MK, Wittmann BM, Brunner AM, Cushman I, Wang Q, et al. CaM kinase kinase beta-mediated activation of the growth regulatory kinase AMPK is required for androgen-dependent migration of prostate cancer cells. Cancer Res 2011;71:528–37.
30. Karacosta LG, Foster BA, Azabdaftari G, Feliciano DM, Edelman AM. A regulatory feedback loop between Ca2+/calmodulin-dependent protein kinase kinase 2 (CaMKK2) and the androgen receptor in prostate cancer progression. J Biol Chem 2012;287:24832–43.
31. Huang YK, Su YF, Lieu AS, Loh JK, Li CY, Wu CH, et al. MiR-1271 regulates glioblastoma cell proliferation and invasion by directly targeting the CAMKK2 gene. Neurosci Lett 2020;737:135289.
32. Gocher AM, Azabdaftari G, Euscher LM, Dai S, Karacosta LG, Franke TF, et al. Akt activation by Ca(2+)/calmodulin-dependent protein kinase kinase 2 (CaMKK2) in ovarian cancer cells. J Biol Chem 2017;292:14188–204.
33. Racioppi L, Nelson ER, Huang W, Mukherjee D, Lawrence SA, Lento W, et al. CaMKK2 in myeloid cells is a key regulator of the immune-suppressive microenvironment in breast cancer. Nat Commun 2019;10:2450.
34. Tojkander S, Ciuba K, Lappalainen P. CaMKK2 regulates mechanosensitive assembly of contractile actin stress fibers. Cell Rep 2018;24:11–9.
35. Kovac B, Teo JL, Makela TP, Vallenius T. Assembly of non-contractile dorsal stress fibers requires alpha-actinin-1 and Rac1 in migrating and spreading cells. J Cell Sci 2013;126(Pt 1):263–73.
36. Davis RT, Blake K, Ma D, Gabra MBI, Hernandez GA, Phung AT, et al. Transcriptional diversity and bioenergetic shift in human breast cancer metastasis revealed by single-cell RNA sequencing. Nat Cell Biol 2020;22:310–20.
37. Lau FH, Vogel K, Luckett JP, Hunt M, Meyer A, Rogers CL, et al. Sandwiched white adipose tissue: a microphysiological system of primary human adipose tissue. Tissue Eng Part C Methods 2018;24:135–45.
38. Scahill SD, Hunt M, Rogers CL, Lau FH. A microphysiologic platform for human fat: sandwiched white adipose tissue. J Vis Exp 2018:57909.
39. Lehmann BD, Bauer JA, Chen X, Sanders ME, Chakravarthy AB, Shyr Y, et al. Identification of human triple-negative breast cancer subtypes and preclinical models for selection of targeted therapies. J Clin Invest 2011;121:2750–67.
40. Wang W, Wyckoff JB, Goswami S, Wang Y, Sidani M, Segall JE, et al. Coordinated regulation of pathways for enhanced cell motility and chemotaxis is conserved in rat and mouse mammary tumors. Cancer Res 2007;67:3505–11.
41. Ramaswamy S, Ross KN, Lander ES, Golub TR. A molecular signature of metastasis in primary solid tumors. Nat Genet 2003;33:49–54.
42. Landemaine T, Jackson A, Bellahcene A, Rucci N, Sin S, Abad BM, et al. A six-gene signature predicting breast cancer lung metastasis. Cancer Res 2008;68:6092–9.
43. Chaffer CL, Weinberg RA. A perspective on cancer cell metastasis. Science 2011;331:1559–64.
44. Hotulainen P, Lappalainen P. Stress fibers are generated by two distinct actin assembly mechanisms in motile cells. J Cell Biol 2006;173:383–94.
45. Soine JR, Brand CA, Stricker J, Oakes PW, Gardel ML, Schwarz US. Model-based traction force microscopy reveals differential tension in cellular actin bundles. PLoS Comput Biol 2015;11:e1004076.
46. Krause M, Gautreau A. Steering cell migration: lamellipodium dynamics and the regulation of directional persistence. Nat Rev Mol Cell Biol 2014;15:577–90.
47. Ridley AJ. Life at the leading edge. Cell 2011;145:1012–22.
48. Butt E, Abel K, Krieger M, Palm D, Hoppe V, Hoppe J, et al. cAMP- and cGMP-dependent protein kinase phosphorylation sites of the focal adhesion vasodilator-stimulated phosphoprotein (VASP) in vitro and in intact human platelets. J Biol Chem 1994;269:14509–17.
49. Harbeck B, Huttelmaier S, Schluter K, Jockusch BM., Illenberger S. Phosphorylation of the vasodilator-stimulated phosphoprotein regulates its interaction with actin. J Biol Chem 2000;275:30817–25.
50. Bachmann C, Fischer L, Walter U, Reinhard M. The EVH2 domain of the vasodilator-stimulated phosphoprotein mediates tetramerization, F-actin binding, and actin bundle formation. J Biol Chem 1999;274:23549–57.
51. Benz PM, Blume C, Seifert S, Wilhelm S, Waschke J, Schuh K, et al. Differential VASP phosphorylation controls remodeling of the actin cytoskeleton. J Cell Sci 2009;122(Pt 21):3954–65.
52. Glass DB. Differential responses of cyclic GMP-dependent and cyclic AMP-dependent protein kinases to synthetic peptide inhibitors. Biochem J 1983;213:159–64.
53. Burkhardt M, Glazova M, Gambaryan S, Vollkommer T, Butt E, Bader B, et al. KT5823 inhibits cGMP-dependent protein kinase activity in vitro but not in intact human platelets and rat mesangial cells. J Biol Chem 2000;275:33536–41.
54. Omori K, Kotera J. Overview of PDEs and their regulation. Circ Res 2007;100:309–27.
55. Baillie GS, Tejeda GS, Kelly MP. Therapeutic targeting of 3',5'-cyclic nucleotide phosphodiesterases: inhibition and beyond. Nat Rev Drug Discov 2019;18:770–96.
56. Snyder PB, Florio VA, Ferguson K, Loughney K. Isolation, expression and analysis of splice variants of a human Ca2+/calmodulin-stimulated phosphodiesterase (PDE1A). Cell Signal 1999;11:535–44.
57. Zhang YS, Li JD, Yan C. An update on vinpocetine: New discoveries and clinical implications. Eur J Pharmacol 2018;819:30–4.
58. Francis SH, Sekhar KR, Ke H, Corbin JD. Inhibition of cyclic nucleotide phosphodiesterases by methylxanthines and related compounds. Handb Exp Pharmacol 2011:93–133.
59. Kloner RA. Cardiovascular effects of the 3 phosphodiesterase-5 inhibitors approved for the treatment of erectile dysfunction. Circulation 2004;110:3149–55.
60. Mattila JT, Thomas AC. Nitric oxide synthase: non-canonical expression patterns. Front Immunol 2014;5:478.
61. Xu W, Liu LZ, Loizidou M, Ahmed M, Charles IG. The role of nitric oxide in cancer. Cell Res 2002;12:311–20.
62. Gupta GP, Massague J. Cancer metastasis: building a framework. Cell 2006;127:679–95.
63. York B, Li F, Lin F, Marcelo KL, Mao J, Dean A, et al. Pharmacological inhibition of CaMKK2 with the selective antagonist STO-609 regresses NAFLD. Sci Rep 2017;7:11793.
64. Davare MA, Saneyoshi T, Soderling TR. Calmodulin-kinases regulate basal and estrogen stimulated medulloblastoma migration via Rac1. J Neurooncol 2011;104:65–82.
65. Bear JE, Svitkina TM, Krause M, Schafer DA, Loureiro JJ, Strasser GA, et al. Antagonism between Ena/VASP proteins and actin filament capping regulates fibroblast motility. Cell 2002;109:509–21.
66. Halbrugge M, Friedrich C, Eigenthaler M, Schanzenbacher P, Walter U. Stoichiometric and reversible phosphorylation of a 46-kDa protein in human platelets in response to cGMP- and cAMP-elevating vasodilators. J Biol Chem 1990;265:3088–93.
67. Rottner K, Behrendt B, Small JV, Wehland J. VASP dynamics during lamellipodia protrusion. Nat Cell Biol 1999;1:321–2.

68. Zuzga DS, Pelta-Heller J, Li P, Bombonati A, Waldman SA, Pitari GM. Phosphorylation of vasodilator-stimulated phosphoprotein Ser239 suppresses filopodia and invadopodia in colon cancer. Int J Cancer 2012;130:2539–48.
69. Chan MH, Aminzai S, Hu T, Taran A, Li S, Kim C, et al. A substitution in cGMP-dependent protein kinase 1 associated with aortic disease induces an active conformation in the absence of cGMP. J Biol Chem 2020;295:10394–405.
70. Deguchi A, Xing SW, Shureiqi I, Yang P, Newman RA, Lippman SM, et al. Activation of protein kinase G up-regulates expression of 15-lipoxygenase-1 in human colon cancer cells. Cancer Res 2005;65:8442–7.
71. Ranek MJ, Kokkonen-Simon KM, Chen A, Dunkerly-Eyring BL, Vera MP, Oeing CU, et al. PKG1-modified TSC2 regulates mTORC1 activity to counter adverse cardiac stress. Nature 2019;566:264–9.
72. Schmoor C, Sauerbrei W, Bastert G, Schumacher M. Role of isolated locoregional recurrence of breast cancer: results of four prospective studies. J Clin Oncol 2000; 18:1696–708.
73. Schmid P, Cortes J, Pusztai L, McArthur H, Kummel S, Bergh J, et al. Pembrolizumab for early triple-negative breast cancer. N Engl J Med 2020; 382:810–21.